European Journal of Medicinal Chemistry xxx (2018) xxx-xxx

Contents lists available at ScienceDirect

European Journal of Medicinal Chemistry

journal homepage: www.elsevier.com

Research paper

Structure-based design and profiling of novel 17β-HSD14 inhibitors

Florian Braun[a, 1], Nicole Bertoletti[a, 1], Gabriele Möller[b], Jerzy Adamski[b, c, d], Martin Frotscher[e], Nathalie Guragossian[f, g], Patrícia Alexandra Madeira Gírio[g], Marc Le Borgne[f], Laurent Ettouati[f], Pierre Falson[g], Sebastian Müller[h], Günther Vollmer[h], Andreas Heine[a], Gerhard Klebe[a], Sandrine Marchais-Oberwinkler[a, *]

[a] Institute for Pharmaceutical Chemistry, Philipps University Marburg, 35032, Marburg, Germany
[b] German Research Center for Environmental Health, Institute of Experimental Genetics, Genome Analysis Center, Helmholtz Zentrum München, 85764, Neuherberg, Germany
[c] Chair of Experimental Genetics, Technical University Munich, 85350, Freising-Weihenstephan, Germany
[d] German Center for Diabetes Research (DZD), 85764, Neuherberg, Germany
[e] Pharmaceutical and Medicinal Chemistry, Saarland University, Campus C23, 66123, Saarbrücken, Germany
[f] Bioactive Molecules and Medicinal Chemistry, EA 4446, Faculty of Pharmacy – ISPB, University Lyon 1, 69373, Lyon, France
[g] Drug Resistance & Membrane Proteins Laboratory, UMR 5086 CNRS-UCBL1, IBCP, 69367, Lyon, France
[h] Chair for Molecular Cell Physiology & Endocrinology, Faculty of Biology, Technical University Dresden, 01062, Dresden, Germany

ARTICLE INFO

Article history:
Received 16 March 2018
Received in revised form 15 May 2018
Accepted 20 May 2018
Available online xxx

Keywords:
17β-Hydroxysteroid dehydrogenase type 14
Inhibitors
Structure-based design
Crystallography

ABSTRACT

The human enzyme 17β-hydroxysteroid dehydrogenase 14 (17β-HSD14) oxidizes the hydroxyl group at position 17 of estradiol and 5-androstenediol using NAD^+ as cofactor. However, the physiological role of the enzyme remains unclear. We recently described the first class of nonsteroidal inhibitors for this enzyme with compound **1** showing a high 17β-HSD14 inhibitory activity. Its crystal structure was used as starting point for a structure-based optimization in this study. The goal was to develop a promising chemical probe to further investigate the enzyme. The newly designed compounds revealed mostly very high inhibition of the enzyme and for seven of them the crystal structures of the corresponding inhibitor-enzyme complexes were resolved. The crystal structures disclosed that a small change in the substitution pattern of the compounds resulted in an alternative binding mode for one inhibitor. The profiling of a set of the most potent inhibitors identified **13** (K_i=9 nM) with a good selectivity profile toward three 17β-HSDs and the estrogen receptor alpha. This inhibitor displayed no cytotoxicity, good solubility, and auspicious predicted bioavailability. Overall, **13** is a highly interesting 17β-HSD14 inhibitor, which might be used as chemical probe for further investigation of the target enzyme.

1. Introduction

17β-hydroxysteroid dehydrogenase type 14 (17β-HSD14), also known as DHRS10 and retSDR3, belongs to the Short-chain Dehydrogenase-Reductase (SDR) superfamily [1,2]. *In vitro,* the human enzyme catalyzes the oxidation at the 17 position of two prominent steroid hormones, estradiol (E2) and 5-androstene-3β,17β-diol (5-diol), in presence of the cofactor NAD^+, thus converting them into their less active analogs, estrone (E1) and dehydroepiandrosterone (DHEA), respectively [2]. However, considering the low turnover of the enzyme for E2 and 5-diol (0.024 and 0.017 min^{-1}, respectively) and the low binding affinity of both substrates (about 6 μM) [3], it is not really clear whether the enzyme is only involved in steroid regulation or contributes to other pathways *in vivo*. The enzyme was described by Sivik et al. [4] to show a broad distribution across various tissues as evaluated by immunohistochemistry studies, while northern blot analyses demonstrated that the enzyme is predominantly expressed in brain, liver, placenta and kidney [2,5]. 17β-HSD14 is a cytosolic enzyme, and its quaternary structure consists of a homotetramer [2,3].

The crystal structures of human 17β-HSD14 in binary complex with NAD^+ (PDB codes: 5JS6 and 5JSF) reveal that the enzyme has a rather lipophilic conical active site, which is narrow in the proximity of the catalytic triad and open to the solvent at the other end [3]. In addition the binding pocket is reduced in size by the penetration of Tyr253′ from an adjacent enzyme monomer of the tetrameric assembly.

The first class of nonsteroidal inhibitors for this enzyme was recently described by us [6]. One of the most promising inhibitors was compound **1** (Fig. 1) [6]. It is a member of the phenyl(6-phenyl)pyridin-2-yl methanone (PPPM) class and exhibits a strong inhibitory effect on the enzyme (K_i = 13 nM). The crystal structure of this inhibitor in complex with the enzyme (PDB code: 5L7Y) shows that the inhibitor adopts a conformation with a complementary shape

* Corresponding author.
Email address: marchais@staff.uni-marburg.de (S. Marchais-Oberwinkler)
[1] F.B. and N.B. contributed equally to the work.

https://doi.org/10.1016/j.ejmech.2018.05.029
0223-5234/

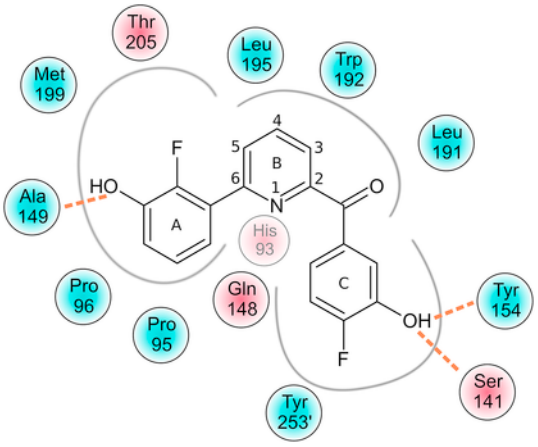

Fig. 1. Schematic representation of the binding mode of compound **1** in the binding pocket of 17β-HSD14. Amino acids with polar functional groups are colored in red. Prevalent hydrophobic amino acids are colored in blue. The different pockets are highlighted with gray lines. H-bonds are depicted as orange dotted lines. (For interpretation of the references to color in this figure legend, the reader is referred to the Web version of this article.)

to the substrate binding pocket, induced by the carbonyl group between the B and the C ring [6]. The compound is bound to the active site via different interactions: The most relevant ones are two strong H-bond contacts between the 3-OH group on the C ring and the catalytic residues Tyr154 and Ser141. Another H-bond interaction between the 3-OH group on the A ring and Ala149 is also observed. The pyridine ring of the inhibitor addresses the hydrophobic pocket formed by Trp192 and Leu195 (Fig. 1).

The goal of this study was to characterize the binding mode of new inhibitors and their interactions with 17β-HSD14 and to optimize the structure of compound **1** in order to develop a promising chemical probe that could be used to further investigate the enzyme.

Structure-based optimization of **1** was first undertaken to extensively exploit potential new interactions provided by the enzyme and thereby enhance the inhibitory activity of the compounds. Then the newly designed compounds were synthesized, tested for 17β-HSD14 inhibition and for seven of them the crystal structures of each corresponding inhibitor-enzyme complex were determined. This structural information was crucial for a better understanding of the structure-activity relationship (SAR), additionally disclosing a shifted binding mode in case of one inhibitor. The profiling of the most potent inhibitors was subsequently initiated: Their selectivity toward three relevant 17β-HSD subtypes and the estrogen receptor alpha (ERα) along with their cytotoxicity and solubility were determined experimentally and their physicochemical properties were calculated.

2. Results and discussion

2.1. Structure-based design of the new inhibitors

The scaffold of compound **1** was used as a starting point for structure-based modifications with the intention to identify the key interactions between the individual inhibitors and the protein and further on to optimize the geometry of the inhibitor **1** for a higher affinity to 17β-HSD14.

Previous studies have shown that in the PPPM class, the interaction of the 3-OH group of the C ring with Tyr154 from the catalytic triad is essential to achieve high inhibitory activity [6]. The increased acidity of the 3-OH function, boosted by the substitution with an adjacent fluorine atom (in *ortho* position to the OH group), correlates with a significant gain in inhibitory activity. Thus, the 3-OH/4-F pattern at the C ring was maintained during the subsequent development process.

In the first optimization strategy **(I)** we focused on the replacement of the linking carbonyl group of **1** (Chart 1), acting as a bridge between the B and C ring. The crystal structure of the protein in complex with **1** disclosed that the carbonyl group is important to induce the overall V-shape of the inhibitor scaffold to perfectly match the architecture of the protein's active site (Fig. 2). Interestingly, the carbonyl group does not form any direct interaction with neighboring amino acids of the protein. Therefore, the role of this linker ("X") was investigated by replacing the carbonyl group with polar linker groups such as an ether oxygen, a secondary amine, or apolar groups such as a tertiary amine and an ethenyl group. The geometry of the modified scaffold (angle between the B and C rings) should be kept similar to that of **1** leaving the positions of the B and C rings virtually unchanged in the protein. Furthermore, amide groups were introduced to enlarge the distance between the B and C ring and to evaluate the consequences of shifting the pyridine B ring in the substrate binding site.

Additionally, a relatively large hydrophobic pocket, next to the B ring in the direction of the exit vectors at the 5 and 6 position of the pyridine core, is observed in the crystal structure of 17β-HSD14 with compound **1** (Fig. 2). Therefore, another optimization strategy **(II)** was selected to address this hydrophobic pocket by extending the pyridine core and fusing the A ring with the B ring resulting in a quinoline-based scaffold. In addition, the rigidity of the quinoline scaffold compared to that of the pyridine-based inhibitors [6] was anticipated to be beneficial for inhibitory activity [7]. Furthermore, the establishment of another scaffold would perhaps give access to compounds with modified pharmacokinetic properties. Hydrophilic and hydrophobic substituents can be introduced in 6 or 7 position of the quinoline moiety, which would enable to explore the chemical space in this region of the binding pocket (Chart 1).

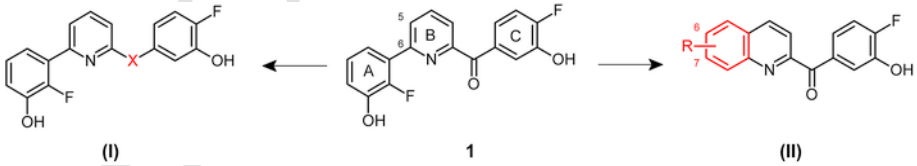

Chart 1. Optimization strategies **(I)** and **(II)** starting from compound **1**.

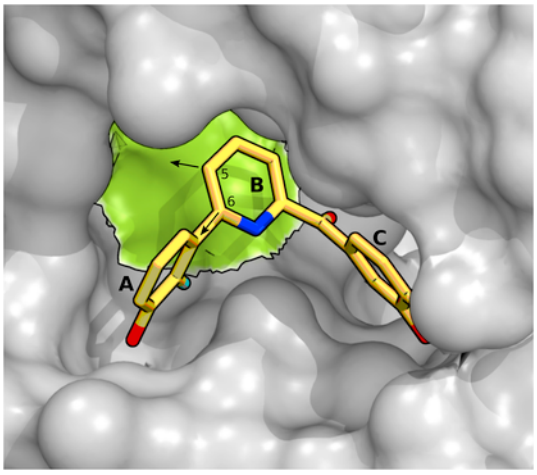

Fig. 2. Close-up view of the binding pocket as formed in the crystal structure of 17β-HSD14 obtained as ternary complex with **1** and NAD^+ (PDB code: 5L7Y) [6]. The protein is displayed in gray by use of the solvent-excluded surface. The inhibitor is shown as stick model. Carbon atoms of the ligand **1** are shown in yellow. The relatively large hydrophobic pocket adjacent to the B ring is highlighted in green. All structural representations were prepared with PyMOL [8]. (For interpretation of the references to color in this figure legend, the reader is referred to the Web version of this article.)

2.2. Pan assay interference compounds

In order to identify undesired compounds, which might bind non-specifically to numerous biological targets, all designed compounds (**2–17**, Tables 1–3) were validated *in silico* using the PAINS-remover computer tool [9,10]. As none of them was assigned as unspecific binder, all were considered for synthesis.

2.3. Physicochemical parameters

Prior to synthesis, the physicochemical properties of all designed compounds (**2–17**, Tables 1–3) were computed to only consider compounds, which match with a good predicted bioavailability profile. The molecular weight was selected to fall into a range of 250–400 g/mol. The *c*log*P*, the total polar surface area (tPSA), the number of rotational bonds and H-bond donors and acceptors were calculated *in silico* and adhered to the Veber Rules [11] and the Lipinski's rule of five [12]. The potential ability of the designed compounds to cross the blood brain barrier (BBB) was also taken into account, as 17β-HSD14 has been reported to be present in the brain [2]. Especially for the pyridine derivatives **1–5** as well as for the quinolines **9**, **11**, **13**, and **17** the physicochemical properties fit well with the profile defined by Pajouhesh and Lenz [13] for compounds showing a good BBB penetration (i.e. MW < 450 g/mol; H-bond donor <3; H-bond acceptor <7; number of rotatable bonds <8; pK_a 7.5–10.5; tPSA <60–70 $Å^2$). The calculated physicochemical parameters and experimentally determined solubilities are summarized in Table S1 (Supporting Information, SI).

2.4. Chemistry

The synthesis of compounds **2–8** was achieved starting from the brominated pyridine derivatives **2c**, **6c**, and **8c** (Scheme 1). The reaction of the 2,6-dibromopyridine **2c** with the phenol derivative **2d** provided **2b** using sodium hydride as base, whereas the reaction with the aniline derivative **3c** afforded the secondary amine **3b** in the presence of lithium hexamethyldisilazane (LHMDS). Activation of carboxylic acids **6d** and **8c** with thionyl chloride and subsequent reaction with the appropriate aniline derivative (**6c** or **3c**) resulted in the amides **6b** and **8b**, respectively. Suzuki coupling reactions [14] of **2b**, **3b**, **6b**, and **8b** with 2-fluoro-3-methoxyphenylboronic acid gave the methoxy intermediates **2a**, **3a**, **6a**, and **8a**. Wittig olefination [15] of

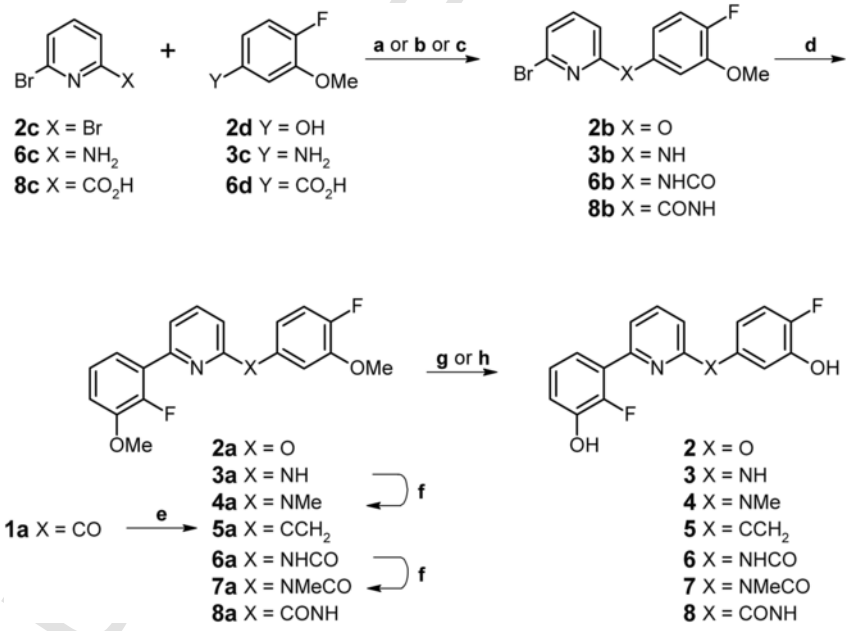

Scheme 1. Synthesis of compounds **2–8**.[a] [a] Reagents and conditions: **a)** for **2b**: **2c**, **2d**, NaH, DMF, 100 °C, overnight; **b)** for **3b**: **2c**, **3c**, LHMDS, 1,4-dioxane/THF 1:1, room temperature, 3 h; **c)** for **6b** (**6c** + **6d**), **8b** (**8c** + **3c**) i) $SOCl_2$, DMF, toluene, reflux, 4 h, ii) Et_3N, DCM, 0 °C to room temperature, overnight; **d)** Cs_2CO_3, $Pd(PPh_3)_4$, 2-fluoro-3-methoxyphenylboronic acid, DME/water (2:1), 80 °C, overnight; **e)** $MePh_3P^+Br^-$, *n*-BuLi, THF, 0 °C to room temperature, overnight; **f)** NaH, MeI, DMF, 0 °C to room temperature, overnight; **g)** for **2–4** and **6–8**, BBr_3, DCM, −80 °C to room temperature, overnight; **h)** for **5**, $BF_3{\cdot}SMe_2$, DCM, room temperature, overnight.

1a [6] with methyltriphenylphosphonium bromide afforded the ethenyl derivative **5a**. Methylation of **3a** and **6a** with methyl iodide using sodium hydride as base provided additionally the methoxy intermediates **4a** and **8a**. The methoxy groups were cleaved with boron tribromide (for compounds **2–4** and **6–8**) or with boron trifluoride dimethylsulfide complex (for compound **5**).

Compounds **9–12** were synthesized in three steps starting from the bromoquinolines **9c**, **11c**, and **12c** and 2-bromonaphthalene (**10c**), respectively (Scheme 2). Lithiation with *n*-butyl lithium and nucleophilic addition to 4-fluoro-3-methoxybenzaldehyde (**9d**) provided after oxidation with 2-iodoxybenzoic acid the ketone intermediates **9a-12a**. Compounds **11c** and **12c** were synthesized by regioselective bromination of the appropriate quinoline *N*-oxides [16]. For compounds **9–11**, the methoxy groups were cleaved with boron tribromide, whereas for **12** boron trifluoride dimethylsulfide complex was used.

The synthesis of compounds **13–17** was enabled starting from precursor **13b** (Scheme 3). For the synthesis of **13b**, 4-bromo-1-fluoro-2-methoxybenzene (**13e**) was used to prepare the corresponding Grignard reagent. The latter was reacted with compound **13d** [17] in a nucleophilic addition and afforded, after oxidation of the formed alcohol with 2-iodoxybenzoic acid, precursor **13b**. The reaction of **13b** with $Zn(CN)_2$ using $Pd(PPh_3)_4$ as catalyst afforded the nitrile **13a** which was subsequently used to prepare the corresponding tetrazole derivative **14a** in a microwave-assisted reaction [18]. Amination of **13b** was performed using similar conditions to the one described by Zeng et al. [19] to afford compound **15a**. Subsequent amide formation using Boc-glycine and HOBt/EDC·HCl as coupling reagents provided compound **16a**. Suzuki coupling of **13b** with 4-methoxy-3-methylphenylboronic acid gave the methoxy intermediate **17a**. All methoxy groups were cleaved with boron tribromide to afford compounds **13–15** and **17**. Compound **16a**, after ether cleavage, was additionally treated with trifluoroacetic acid to afford **16** as trifluoroacetate salt.

2.5. Biological evaluation of 17β-HSD14 inhibitory activity

The inhibitory activities of the synthesized compounds were evaluated by means of a fluorescence-based assay, quantifying the fluorescence of NADH produced during the catalytic reaction. The assay was carried out as already reported [3,6], using the purified, recombinantly expressed enzyme, E2 as substrate, NAD^+ as cofactor, and the inhibitors. Percentages of inhibition (measured at an inhibitor concentration of 2 μM) as well as binding affinities (K_i) were determined. For **9a**, no K_i could be measured due to its limited solubility. Thus, its inhibitory activity was expressed as percentage of inhibition at the highest soluble concentration of the inhibitor (100 μM).

Starting from inhibitor **1**, the linker between the B and the C ring was investigated following our first optimization strategy concept by replacing the carbonyl group with different functional groups. Ether **2** (K_i = 58 nM), amine **3** (K_i = 47 nM), and methylamine **4** (K_i = 42 nM) were shown to be equipotent ligands with slightly decreased affinity compared to **1** (K_i = 13 nM). The introduction of an ethenyl group resulted in a ten times more potent inhibitor **5** (K_i = 1.5 nM), whereas the presence of an amide linker led to a strong decrease in inhibitory activity (**6**: K_i = 686 nM, **8**: K_i = 336 nM) and the methylated amide (**7**: K_i = 2030 nM) was even detrimental for 17β-HSD14 inhibition compared to **1** (Table 1).

In the second approach the pyridine B ring of compound **1** (K_i = 13 nM) was expanded and led to the equipotent quinoline-based inhibitor **9** (K_i = 12 nM, Table 2). The presence of the 3-OMe group at the C ring (**9a**, no inhibition at 2 μM; 21% inhibition at 100 μM) was detrimental for the inhibitory activity when compared to the 3-OH analog **9** (69% inhibition at 2 μM). The role of the nitrogen atom of the quinoline moiety with respect to the inhibitory activity was further investigated by the synthesis of the naphthalene derivative **10** (K_i = 6 nM), which was shown to have a similar inhibition constant as the quinoline analog **9**. The nitrogen might not establish

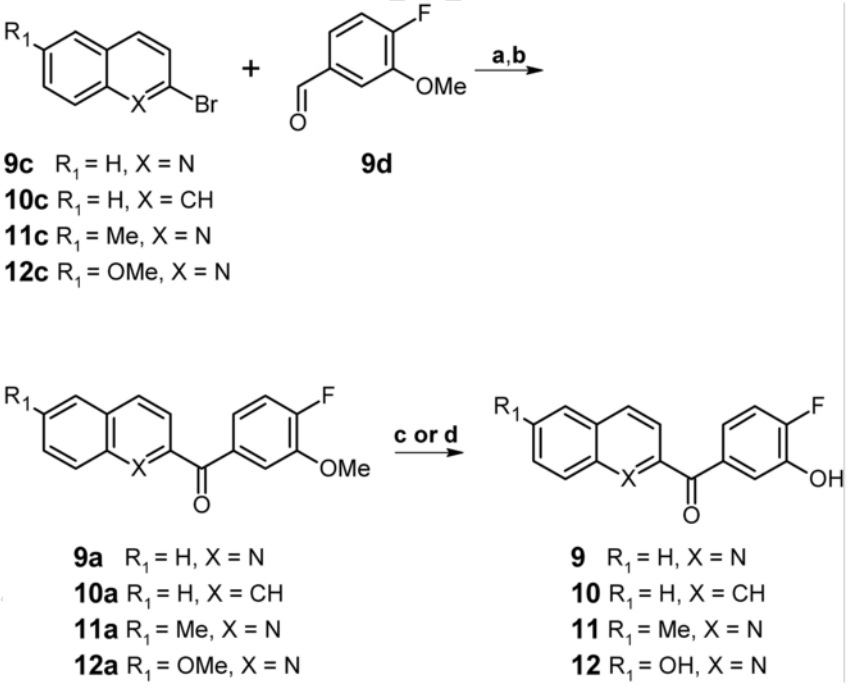

Scheme 2. Synthesis of compounds **9–12**.[a] [a] Reagents and conditions: **a)** *n*-BuLi, anhydrous THF, −80 °C to room temperature, 2 h; **b)** 2-iodoxybenzoic acid, anhydrous THF, 60 °C, 2 h; **c)** for **9–11**, BBr_3, DCM, −80 °C to room temperature, overnight; **d)** for **12**, $BF_3.SMe_2$, DCM, room temperature, overnight.

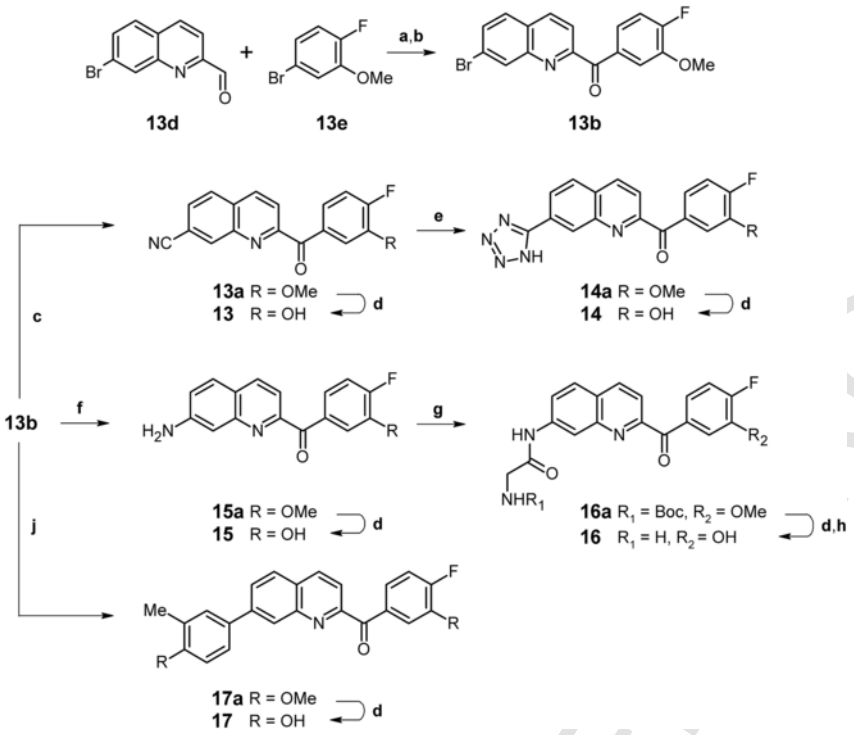

Scheme 3. Synthesis of compounds **13–17**.[a] [a] Reagents and conditions: **a)** Mg, anhydrous THF, 60 °C, 2 h, 80 °C, 4 h; **b)** 2-iodoxybenzoic acid, anhydrous THF, 60 °C, overnight; **c)** $Zn(CN)_2$, $Pd(PPh_3)_4$, DMF, 120 °C, 3 h; **d)** BBr_3, DCM, −80 °C to room temperature, overnight; **e)** NaN_3, NH_4Cl, DMF, microwave irradiation, 30 W, reflux (open vessel), 30 min; **f)** CuI, NH_4OH, L-Proline, K_2CO_3, DMSO, 85 °C, 15 h; **g)** Boc-Gly-OH, HOBt, EDC·HCl, DIPEA, DCM, 40 °C; **h)** TFA, DCM, 1 h, room temperature; **j)** Cs_2CO_3, $Pd(PPh_3)_4$, 4-methoxy-3-methylphenylboronic acid, DME/water (2:1), 80 °C, overnight.

Table 1
17β-HSD14 inhibition constant (K_i) of pyridine derivatives with different linkers between the B and C ring.

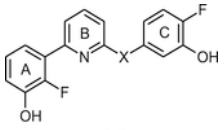

1-8

compd	X	17β-HSD14 K_i (nM)[a]
1	C=O	13 ± 5
2	O	58 ± 12
3	NH	47 ± 7
4	NMe	42 ± 8
5	$C=CH_2$	1.5 ± 0.4
6	NHCO	686 ± 54
7	NMeCO	2030 ± 180
8	CONH	336 ± 54

[a] Recombinantly expressed, purified 17β-HSD14 enzyme, fluorimetric assay, [E2] = 32 µM, [NAD^+] = 1.2 mM, 25 °C. Mean and SD values of at least three independent experiments each with three technical repeats.

Table 2
17β-HSD14 inhibition constant (K_i) of quinoline and naphthalene derivatives.

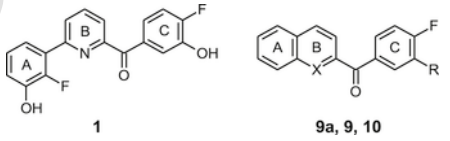

1 **9a, 9, 10**

Compd	X	R	17β-HSD14 K_i (nM)[a]
1	–	–	13 ± 5
9a	N	OMe	21%[b]
9	N	OH	12 ± 3, (69%)[c]
10	CH	OH	6 ± 2

[a] Recombinantly expressed, purified 17β-HSD14 enzyme, fluorimetric assay, [E2] = 32 µM, [NAD^+] = 1.2 mM, 25 °C. Mean and SD values of at least three independent experiments each with three technical repeats.

[b] Percent inhibition at 100 µM, standard deviation <10%.

[c] Percent inhibition at 2 µM, standard deviation <10%.

any specific interaction with the protein, however, it enhances the solubility of the **9** over its naphthalene analog **10** (~four times, Table S1, SI).

Furthermore, compound **9** (K_i = 12 nM) was decorated with different substituents in 6 or 7 position of the quinoline moiety. A methyl group in 6 position (**11**: K_i = 6 nM) did not influence the inhibition, whereas a hydrophilic OH-group (compound **12**, K_i = 119 nM) reduced the potency ten times compared to that of **9**. In 7 position, the introduction of non-hydrophilic substituents (**13**: K_i = 9 nM; **17**: K_i = 6 nM) as well as polar substituents (**14**: K_i = 10 nM; **15**: K_i = 34 nM; **16**: K_i = 23 nM) resulted in inhibitors with similar potencies compared to **9** (Table 3).

2.6. Crystal structures determination

Inhibitors of both, the pyridine and the quinoline series, showing the best inhibitory activity for 17β-HSD14, were selected for crystallization. Seven inhibitors could be co-crystallized in complex with the protein resulting in crystals of sufficient quality for structure determination (**2**, PDB code: 5O6O; **4**, PDB code: 5O43; **5**, PDB code: 5O42; **9**, PDB code: 5O6Z; **11**, PDB code: 5O6X; **13**, PDB code: 5O7C and **16**, PDB code: 5O72). All crystals exhibited tetragonal symmetry in space group (*I*422) with the asymmetric unit formed by

Table 3
17β-HSD14 inhibition constant (K_i) of 6- and 7-substituted quinoline derivatives.

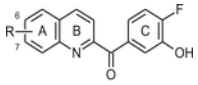

9-17

compd	R	17β-HSD14 K_i (nM)[a]
9	H	12±3
11	6-Me	6±2
12	6-OH	119±7
13	7-CN	9±1
14	7-(tetrazol-5-yl)	10±2
15	7-NH_2	34±7
16	7-NHGly	23±2
17	7-(4-hydroxy-3-methylphenyl)	6±2

[a] Recombinantly expressed, purified 17β-HSD14 enzyme, fluorimetric assay, [E2]=32 µM, [NAD^+]=1.2 mM, 25 °C. Mean and SD values of at least three independent experiments each with three technical repeats.

only one monomer, which assembled with the other three symmetry equivalent molecules to form the biological relevant homotetramer. This was in accordance with the findings of our previous study [3]. The structures obtained have a resolution ranging between 1.35 Å to 1.91 Å. Data collection, processing and refinement statistics can be found in Table S2A and B (SI).

2.7. Binding mode of the pyridine-based inhibitors in complex with 17β-HSD14 and SAR study

The superimposition of the crystal structures of the enzyme in ternary complexes with the pyridine-based inhibitors **2**, **4** and **5** revealed that these three inhibitors, despite a chemically varied linker between the C and the B ring, bind in a similar mode as **1** (Fig. 3A). All inhibitors, in spite of their different linkers, adopt the same V-shaped conformation as observed for **1**. For all three crystallized inhibitors, the same conserved water molecule (W1) is found at the same position as described for the other known pyridine-based inhibitors [6]. As expected, the ether oxygen (**2**, Fig. 3B) is not involved in any direct interaction with the protein. The methyl amine

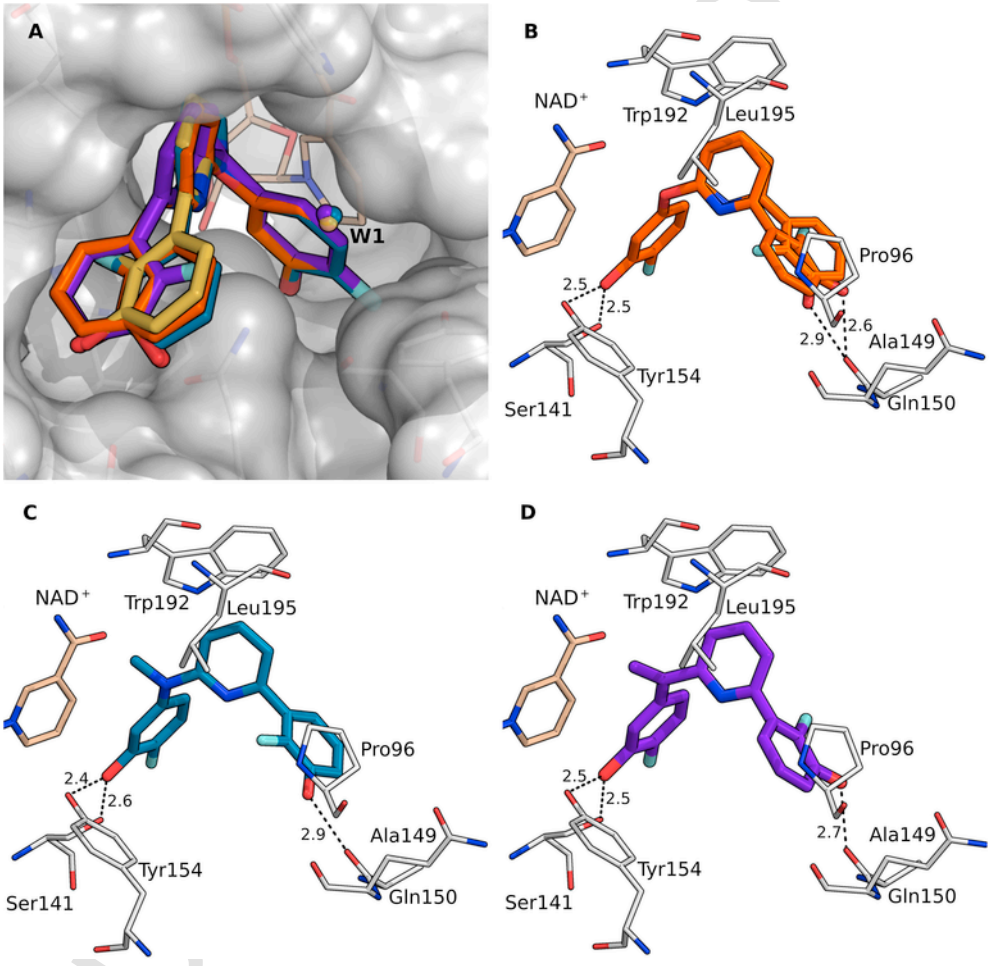

Fig. 3. Close-up view of the binding pocket of the four crystal structures of 17β-HSD14 obtained as ternary complexes with NAD^+ and the pyridine-based inhibitors: **1** (PDB code: 5L7Y, A) [6], **2** (PDB code: 5O6O, A and B), **4** (PDB code: 5O43, A and C), and **5** (PDB code: 5O42, A and D). The carbon atoms of the ligands are shown for **1** in yellow, **2** in orange (two conformers), **4** in blue, **5** in purple and NAD^+ in light beige. (A) Superimposition of the four crystal structures. The protein is displayed in gray by use of the solvent-excluded surface. Inhibitors and cofactor are shown as stick models. The individual sites of the water molecule W1 are represented in the same color as the corresponding inhibitor in the various structures. W1 corresponds to water molecule 508 in 5L7Y, 472 in 5O43, 488 in 5O42 and 501 in 5O6O (hidden behind the other water molecules) in the respective crystal structures. In panels B, C and D, the amino acids within a distance of 4.6 Å are shown as thin lines with the carbon atoms in white. H-bond interactions are depicted as dotted lines. Distances are given in Å. (For interpretation of the references to color in this figure legend, the reader is referred to the Web version of this article.)

(**4**, Fig. 3C) and the ethylene moiety (**5**, Fig. 3D) accommodate well in the hydrophobic pocket formed by Leu191, Trp192 and Leu195 (amino acids shown in Fig. 1). The enhanced flexibility of the ligand with the ether linker is reflected in the split conformation of the A and B ring of **2** (Fig. 3B). Remarkably, the slightly different valence angle between the B and C ring (~1°) generated by the ethylene linker when compared to the respective angle in **1** pushes the B ring of **5** into the direction of Leu195 leading to a flip of the A ring plane of about 180° and resulting in an orientation of the OH and F substituents in opposite direction to that in compound **1** (Fig. 3A). The 3-OH group at the A ring of all the inhibitors is within H-bond distance to the carbonyl backbone of Ala149 (d = 2.7–2.9 Å).

Replacement of the carbonyl moiety (**1**) for the ethylene group (**5**) led to an almost ten-fold more potent inhibitory compound **5** (K_i = 1.5 nM) compared to **1** (K_i = 13 nM). The crystal structure of **5** revealed that the ethylene linker is more deeply buried in the hydrophobic pocket defined by Leu191, Leu195 and Trp192 compared to the carbonyl group. This linker is also beneficial for binding due to its lower desolvation penalty compared to the carbonyl analog **1** whose polar oxygen is not involved in any interaction at the protein binding site. The flipped A ring of **5** (compared to **1**) led to an improved geometry because this ring comes into proximity to the hydrophobic region formed by Pro95, Pro96 and Leu195 (van der Waals interactions). In addition, the 3-OH group attached to the A ring is moved to a more favorable H-bond distance (d = 2.7 Å) toward the carbonyl group of the Ala149 backbone. All together these aspects might be responsible for the gain in 17β-HSD14 inhibitory activity of **5** compared to **1**. Compounds **6**, **7**, and **8** lose affinity possibly owing to the introduced polar amide linkers, which remain exposed to a predominantly hydrophobic environment. In addition, the A rings of these inhibitors become partly solvent exposed, most probably due to the fact that the compounds are rather long for the binding site, resulting in the loss of interactions of the A ring with the protein. Furthermore, the important V-shape of these inhibitors **6**, **7**, and **8** could not be achieved.

2.8. Binding mode of the quinoline-based inhibitors in complex with 17β-HSD14 and SAR study

From the crystal structures of **9**, **13** and **16** (Fig. 4), it became apparent that all these ligands adopted the same binding mode. In addition, the C rings of the three quinoline-based inhibitors **9**, **13**, and **16** are located in the same region compared to the C ring of pyridine-based inhibitors described so far: The 3-OH group of the C ring experiences H-bond interactions with the catalytic Tyr154 (d = 2.4–2.5 Å) and Ser141 (d = 2.4–2.5 Å) (Fig. 4A and B and Fig. 5). The quinoline core addresses the hydrophobic region formed by Pro95, Pro96, Leu191, Trp192 and Leu195 (amino acids shown in Fig. 1). The primary amine substituent of **16** is in H-bond distance with the carbonyl group of the side chain of Gln150 (d = 2.9 Å), while no interaction with the protein can be observed for the nitrile substituent of **13**. These three inhibitors showed high inhibition of the enzyme (K_i = 12 nM, 9 nM and 23 nM for **9**, **13** **16**, respectively) in the same range as the pyridine derivatives. The additional hydrophobic interactions of the quinoline core motif with the pocket formed by Leu191, Trp192, Leu195 and Met199 may have compensated the loss of the A ring and the H-bond interactions with Ala149, which were observed for compound **1** (e.g. **9**: K_i = 12 nM *vs.* **1**: K_i = 13 nM). The conserved water molecule W1 is present in a similar position as described for the pyridine-based inhibitors.

As already remarked in our previous work [6], replacing the 3-OH group at the C ring by a 3-OMe moiety resulted in a strong drop of the inhibitory activity (**9a**, 21% inhibition at 100 μM), certainly due to the missing H-bond interaction with the catalytic Tyr154.

No crystal structure could be obtained for inhibitors **14**, **15**, **12** and **17** in complex with 17β-HSD14 and NAD^+. A model structure can provide insight on the interactions achieved by a ligand with the protein and therefore can sustain the understanding of SAR studies. First to validate the method, the quinoline-based inhibitor **9** was modeled into the crystal structure of **1**. The simulation suggested a binding mode for **9**, which was identical to the co-crystal structure (Fig. S3, SI), validating the model structure. A model structure was created for **14**, **15**, and **17**. From their simulations, these ligands are not expected to perform any additional interaction compared to **9** (Fig. S4A–D, SI). The 6-OH group of **12** is located in a lipophilic environment, which is unfavorable. The predicted interactions made by the ligands **12**, **14**, **15**, and **17**, as observed in the different models, correlate well with their respective inhibition constant (K_i = 119 nM, 10 nM, 34 nM, 6 nM, and 12 nM for **12**, **14**, **15**, **17**, and **9** respectively).

The crystal structure of compound **11** displays a deviating binding mode for this ligand when compared to the other inhibitors described previously (Fig. 4C). The entire compound is pushed deeper into the active site and induces an altered conformation of the sidechain of Tyr253′ of the neighboring monomer of the tetramer. The C ring of **11** is stacked behind Tyr253'. The 3-OH group of the C ring remains

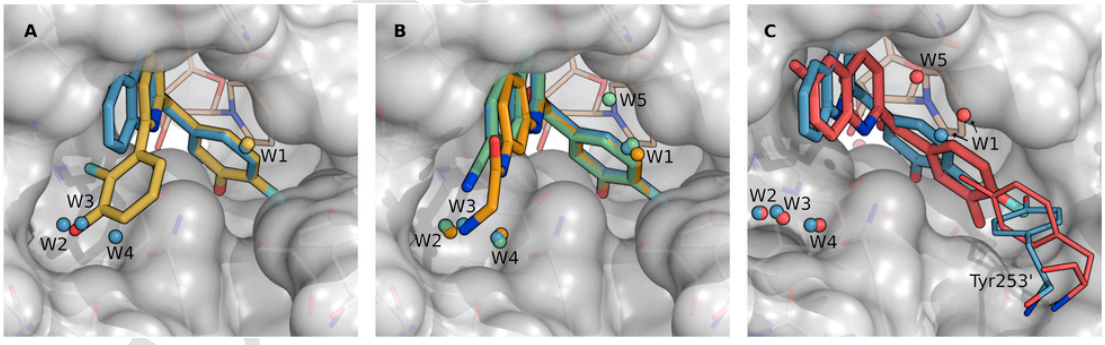

Fig. 4. Close-up view of the binding pocket of the superimposed crystal structures of 17β-HSD14 obtained in ternary complexes with NAD^+ and different inhibitors. The protein is displayed in gray by use of the solvent-excluded surface. Inhibitors and cofactor are shown as stick models. The carbon atoms of the NAD^+ are shown in light beige. The water molecules W1-W5 are represented in the same color as the corresponding inhibitor of the individual structures. (A) The carbon atoms of the ligands are shown for **1** (PDB code: 5L7Y) [6] in yellow and **9** (PDB code: 5O6Z) in blue. (B) The carbon atoms of the ligands are shown for **9** in blue, **13** (PDB code: 5O7C) in green and **16** (PDB code: 5O72) in light orange. (C) The carbon atoms of the ligands are shown for **9** in blue and **11** (PDB code: 5O6X) in red. (For interpretation of the references to color in this figure legend, the reader is referred to the Web version of this article.)

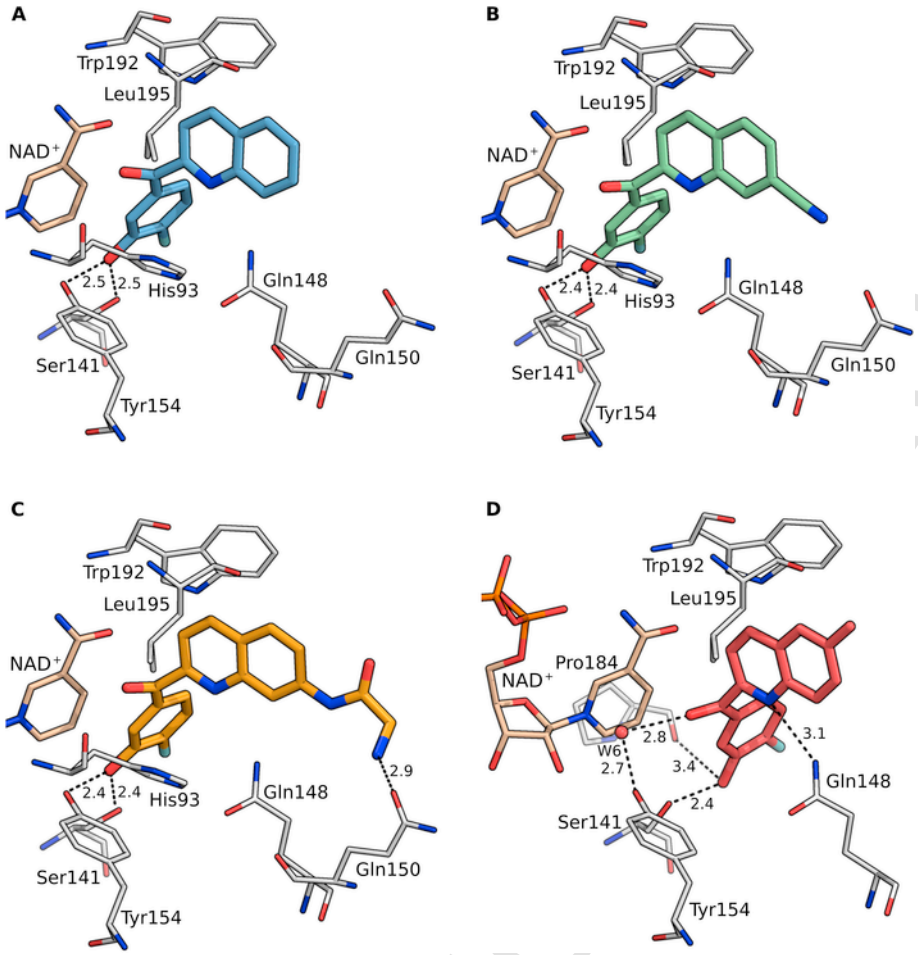

Fig. 5. Close-up view of the binding pockets of the crystal structures of 17β-HSD14 in complex with cofactor NAD^+ and inhibitors. The carbon atoms are shown in blue for **9** (A, PDB code: 5O6Z), green for **13** (B, PDB code: 5O7C), light orange for **16** (C, PDB code: 5O72) and red for **11** (D, PDB code: 5O6X). The inhibitors and cofactor NAD^+ are shown as stick models. The amino acids are shown as thin lines with carbon atoms in white. The water molecule W6 is represented as red sphere. W6 corresponds to water molecule 419 in 5O6X. H-bonds interactions are depicted as dotted lines. Distances are given in Å. (For interpretation of the references to color in this figure legend, the reader is referred to the Web version of this article.)

within H-bond distance to the side chain OH group of the catalytic Ser141 (d = 2.4 Å). Furthermore, the 3-OH group of the C ring is also in H-bond distance with the carbonyl group of the backbone of Pro184 (d = 3.4 Å). However, the important and direct H-bond contact between this 3-OH group and the side chain of Tyr154, found in all other structures of 17β-HSD14 in complex with inhibitors, is not present anymore. Instead, the carbonyl group of the ligand interacts with Tyr154 mediated via the water molecule W6 (d = 2.7 and 2.8 Å). The 6-methylquinoline moiety is completely buried in the hydrophobic pocket composed of Pro95, Pro96, Leu191, Trp192 and Leu195 and, in addition, the quinoline nitrogen is within H-bond distance to the sidechain of Gln148 (d = 3.1 Å, Fig. 5D). This deviating binding mode might result from steric repulsion of the added methyl group in position 6 with Met199 of the protein, which pushes the ligand deeper into the active site of the enzyme. In the position described, the methylated quinoline moiety is able to form optimum hydrophobic interactions with the pocket formed by Leu191, Tpr192, Leu195, Met199 and Thr205 (Fig. 5). As the deviating binding mode of the 6-methylquinoline derivative **11** did not parallel a significant change in inhibition strength compared to **9** (K_i = 6 nM *vs*. K_i = 13 nM, respectively), the cumulative hydrophobic effects and the new interaction with water W6 seem to compensate the loss in the direct interaction to Tyr154.

Interestingly, the water molecule W6 is entrapped to mediate a contact between ligand and protein. This water is also found at the same position in the 17β-HSD14-NAD^+ complex structures with **11** and **13** and in the 17β-HSD14 holoenzyme complex with NAD^+ (PDB code: 5JSF (S205 variant) and 5JS6 (T205 variant), Fig. 7).

In the case of the protein complex with **11**, the water molecule W1 is shifted upward due to the different conformation of this inhibitor (Fig. 4C). To be remarked, three additional conserved water molecules (W2-W4) can be observed in the structures of **9**, **13**, **16**, and **11**, located in the pocket usually occupied by the A ring of the pyridine-based inhibitors (Fig. 4). In case of the complex with **16**, one water molecule (W3) is displaced by the amino group of the glycine moiety of the inhibitor.

Compounds **9** and **11** differ only in the presence/absence of a methyl group at position 6 of the quinoline ring. Their crystal structures in complex with the protein reveal that these two compounds are stabilized by the protein via different interactions. This result was unexpected and highlights how difficult it is to predict the binding mode of a compound using docking studies in case of highly flexible proteins.

2.9. Comparison of the structures of 17β-HSD14 and 17β-HSD10

17β-HSD10 and 17β-HSD14 share the highest sequence identity between the protein members of the 17β-HSD family (27.5% as calculated with Cluster omega program from the UniProt database [20]). Therefore, the selectivity aspect towards 17β-HSD10 should be taken into account for the designed 17β-HSD14 inhibitors.

The crystal structure of the 17β-HSD10 (PDB code: 1U7T [21]) has been reported in complex with the inhibitor **AG18051** [21], which is covalently linked to the cofactor NAD^+ (**NAD-AG18051** adduct) and can be compared to the 17β-HSD14 in complex with the pyridine-based inhibitor **1** (PDB code: 5L7Y [6], Fig. 6).

Structural comparison of the Rossman-fold region between the two enzymes reveals that the cofactor is found with a nearly identical geometry in the pocket, with a RMSD value of 0.6 Å after alignment of the Cα of the protein (calculated with fconv [22]). The structure of the substrate binding site deviates among both enzymes, although the position of the catalytic triad is preserved. The flexible loop of 17β-HSD14 (αFG1 and αFG2 segments) is slightly longer than the one corresponding to 17β-HSD10. In addition, 17β-HSD10 bears a solvent-exposed loop (L_D loop, residues 94–114, Fig. 6), which is essential for the interaction of 17β-HSD10 with β-amyloid-protein (Aβ) [23] and does not exist in 17β-HSD14. In both 17β-HSD10 and 17β-HSD14, the C-terminal tail is unstructured. However, in the case of 17β-HSD14, the C-terminal tail is involved in the interactions between two monomers. Moreover, His93 and Gln148 induce the V-shaping of the substrate binding site of 17β-HSD14. For type 10, His93 is replaced by Ala95 and as consequence Gln162 (corresponding to Gln148 for 17β-HSD14) is flipped to the outer side of the binding pocket while the side chain of Gln165 in 17β-HSD10 is oriented toward the center of the binding pocket. Taken together, these facts result in a shallower binding pocket for 17β-HSD10 compared to the one of type 14. The inhibitors **1** and **AG18051** occupy a similar region in type 14 and 10, respectively. However, the inhibitor for 17β-HSD10 adopts a rather planar geometry, reinforced by the hydrophobic residues Leu206 and Leu209 (Fig. 6).

2.10. Selectivity toward 17β-HSD1, 17β-HSD2 and 17β-HSD10

The reference compound **1**, used as the starting point of this study, was retrieved from a library of known 17β-HSD1 and 17β-HSD2 inhibitors [24,25]. It was therefore important to validate whether the preference for binding to 17β-HSD1 and 17β-HSD2 of the new inhibitors was maintained or whether the optimized compounds showed good selectivity profiles in favor of 17β-HSD14. In addition, as mentioned previously, the investigation of the selectivity profile with respect to binding to 17β-HSD10 is of high concern considering the high sequence identity between 17β-HSD 10 and 17β-HSD 14 enzymes.

We selected inhibitors that displayed good inhibitory activity for 17β-HSD14 ($K_i < 100$ nM) to validate their selectivity profile toward 17β-HSD1, 17β-HSD2, and 17β-HSD10. The ability of the selected 14 inhibitors to inhibit these enzymes was studied using a competitive assay, by quantifying the formation of [^{3}H]-E2 (for 17β-HSD1) and [^{3}H]-E1 (for 17β-HSD2 and 10) after incubation of the protein

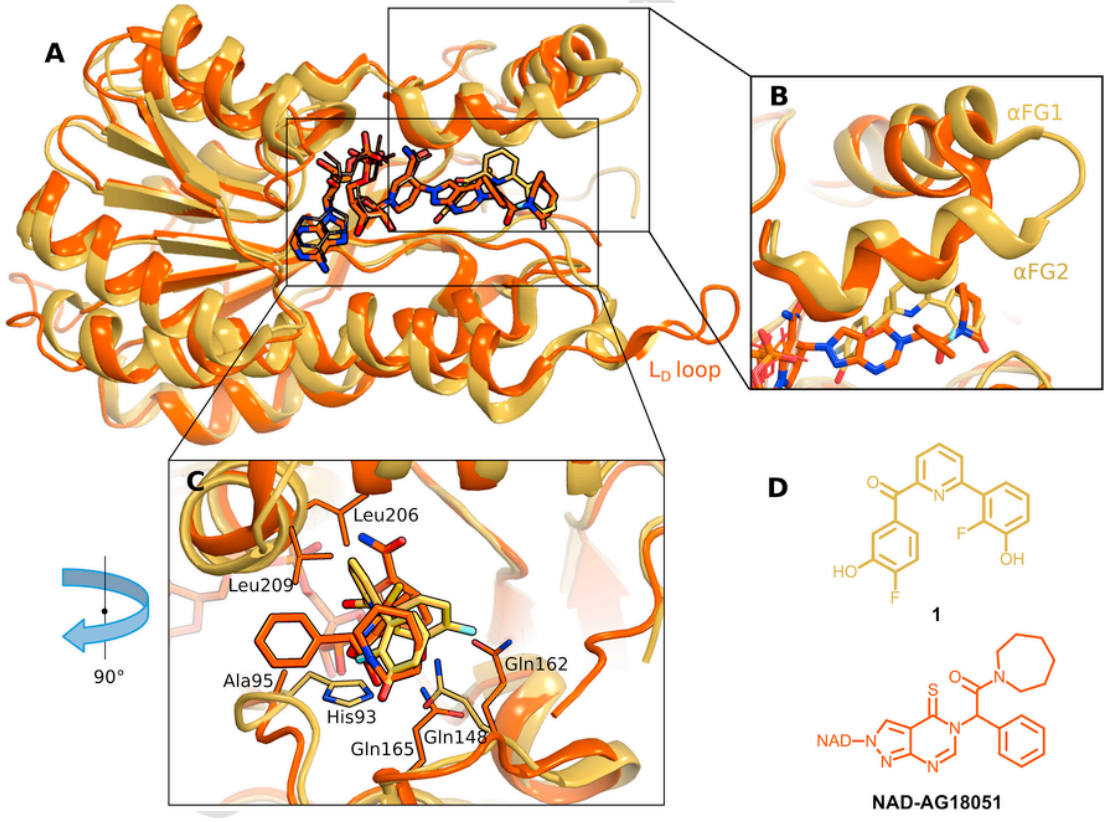

Fig. 6. Superimposition of the 17β-HSD14 (yellow, PDB code: 5L7Y) and 17β-HSD10 (orange, PDB code: 1U7T) structures. The proteins are shown as ribbon models. The ligands and cofactors are shown as stick models and their carbon atoms are colored as the corresponding protein structure. (**A**) Overview of the complexes structures. (**B**) Close-up view on the flexible loops of 17β-HSD10 and 17β-HSD14 (αFG1 and αFG2). (**C**) Close-up view on the ligand binding pockets. (**D**) Chemical structures of inhibitor **1** and the **NAD-AG18051** adduct. (For interpretation of the references to color in this figure legend, the reader is referred to the Web version of this article.)

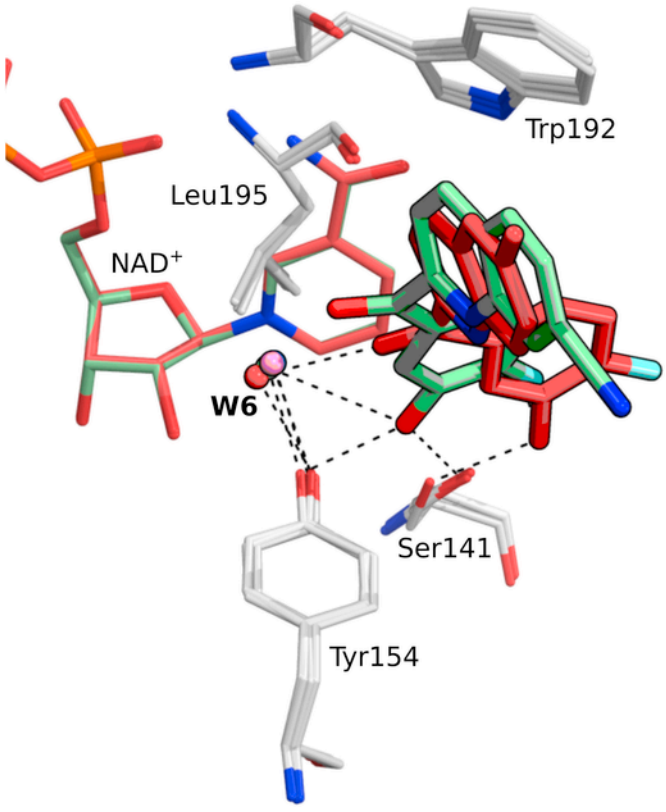

Fig. 7. Superimposition of the crystal structures of the 17β-HSD14 in complex with the cofactor NAD^+ (PDB code: 5JSF (S205 variant) and 5JS6 (T205 variant)) and 17β-HSD14 in complex with NAD^+ and the inhibitors **11** (PDB code: 5O6X) and **13** (PDB code: 5O7C). The carbon atoms of **13** are colored in green and those of **11** in red. The inhibitors and cofactor NAD^+ are shown as stick models. The amino acids are shown as thin lines with carbon atoms in white. H-bonds are depicted as dotted lines. The water molecule W6 is represented in red for 5O6X, in pink for 5JS6, in green for 5O7C and in blue for 5JSF, and corresponds to water molecule number 419, 424, 403 and 439, respectively, in the different crystal structures. The latter two water molecules are hidden by the other two waters in the superimposition of the four structures. (For interpretation of the references to color in this figure legend, the reader is referred to the Web version of this article.)

with labeled substrate, cofactor, and inhibitors [26]. The results of these assays are shown in Table 4 and expressed as percentage of inhibition.

2.10.1. Selectivity of the pyridine derivatives

The first approach to modify the scaffold of the pyridine derivatives resulted in the production of less selective compounds (**2–5**), which showed even higher inhibition of 17β-HSD1 (57–99% 17β-HSD1 inhibition at 1 μM) and of 17β-HSD2 (82–100% 17β-HSD2 inhibition at 1 μM) compared to the initial compound **1** (8% 17β-HSD1 inhibition and 56% 17β-HSD2 inhibition, both measurements at 1 μM).

The ethylene linker derivative **5** is highly active on 17β-HSD1 (88% at 1 μM) and 17β-HSD14 (K_i = 1.5 nM) while the carbonyl linker derivative **1** is inactive on 17β-HSD1 (8% at 1 μM) but highly active on 17β-HSD14 (K_i = 13 nM). It is striking that a minimal change in the structure of the inhibitor leads to such a difference in 17β-HSD1 inhibitory activity and has no influence on 17β-HSD14 activity taking into account that both enzymes can bind the same substrate/product. A rational explanation for the observed selectivity profile of the inhibitors toward 17β-HSD1 and 17β-HSD2 in structural terms appears rather difficult to establish. Due to the conformational properties of the 17β-HSD1 binding pocket - with the flexible loop restricting the remote part opposite to the catalytic triad, and the existence of several conformations of the flexible loop [6]- it is extremely challenging to perform reliable docking studies. However, it can be imagined that the pyridine derivatives do not bind in the same way to 17β-HSD1 and to 17β-HSD14, leading to differences in the inhibitory activities. The lack of a crystal structure of 17β-HSD2 does not allow a detailed conclusive comparison.

Table 4
17β-HSD1, 17β-HSD2, and 17β-HSD10 inhibitory activities of the most interesting compounds.

compd	17β-HSD1% inh. at 1 μM[a]	17β-HSD2% inh. at 1 μM[b]	17β-HSD10% inh. at 1 μM[c]
1	8	56	n.i.
2	69	100	17
3	57	82	n.i.
4	99	100	19
5	88	100	n.i.
9	6	76	n.i.
10	64	96	n.i.
11	12	78	n.i.
12	20	71	n.i.
13	n.i.	56	n.i.
14	n.i.	52	n.i.
15	21	83	n.i.
16	3	63	n.i.
17	11	80	n.i.

[a] Placental 17β-HSD1 enzyme, cytosolic fraction, substrate [^{3}H-E1 + E1] = 500 nM, [NADH] = 0.5 mM, mean value of two determinations; standard deviation < 10%, n i.: no inhibition.

[b] Placental 17β-HSD2 enzyme, microsomal fraction, substrate [^{3}H-E2 + E2] = 500 nM, [NAD^+] = 1.5 mM, mean value of two determinations; standard deviation < 10%.

[c] Recombinantly expressed 17β-HSD10 enzyme, bacterial suspension, substrate [^{3}H-E2] = 25 nM, [NAD^+] = 0.75 mM, mean value of three determinations; standard deviation < 10%, n i.: no inhibition.

With respect to 17β-HSD10, only compounds **2** and **4** showed a weak inhibitory activity (17% and 19% inhibition at 1 μM, respectively) while all the other synthesized derivatives were inactive suggesting an overall very convincing selectivity profile toward 17β-HSD10 (Table 4). This selectivity might be explained by the rather flat geometry of the active site of 17β-HSD10, which clashes with our V-shaped inhibitors.

Taking together the activity and selectivity profile of the pyridine derivatives, it appeared reasonable to focus further investigations on the quinoline class with the methanone linker.

2.10.2. Selectivity of the quinoline derivatives

The quinoline-based compounds **9–17**, obtained from the second optimization strategy, resulted in inhibitors which showed no significant 17β-HSD1 inhibitory activity at 1 μM. Only the naphthalene derivative **10** fell out of this profile and exhibited higher 17β-HSD1 inhibitory activity (64% inhibition at 1 μM).

A direct comparison of the 17β-HSD1 and 17β-HSD2 inhibitory activities with those of 17β-HSD14 is problematic as the assays were performed using different conditions. However in our previous study, an 17β-HSD2 IC_{50} of 1 μM was assessed for compound **1** [6]. Taking into account the kinetic constant of the assay (K_m = 403 nM [27], substrate concentration = 500 nM), a calculated K_i (cK_i) for **1** can be estimated to be about 450 nM using the Cheng-Prusoff equation [28]. The determined K_i for **1** in the 17β-HSD14 assay was 13 nM. Compound **1** is therefore about 35-fold more selective for 17β-HSD14 compared to 17β-HSD2. As compounds **13**, **14**, and **16** exhibited a 17β-HSD2 inhibition in the same range as **1** (52–63% inhibition at

1 μM), it can be expected that they will be as selective as **1** toward 17β-HSD2, thus underlining the satisfactory selectivity discrimination of the quinoline-based inhibitors against 17β-HSD1 and 17β-HSD2.

The affinity of quinoline-based inhibitors toward 17β-HSD10 was minor. Similar to the pyridine derivatives, the selectivity toward 17β-HSD10 might be explained by the quite flat active site geometry of the enzyme. It certainly does not accept kinked inhibitors, even if the angular shape of the quinoline-based compound is less pronounced than the V-shape of the pyridines-based analogs.

Taken all together, inhibitors **13**, **14**, and **16** show a good selectivity profile toward 17β-HSD1, 17β-HSD2 and 17β-HSD10 exhibiting signatures comparable to that of the pyridine-based **1**.

2.11. Stimulation of the estrogen receptor alpha (ERα)

The synthesized compounds are structurally derived from **1**, which is a steroidomimetic (mimic of estradiol). Estradiol is known to induce cell proliferation upon binding to the ERα in the estrogen sensitive organs like the breast or the endometrium. It should therefore be verified if the newly synthesized compounds might show undesired effects by activating the ERα, which would complicate the interpretation of an *in vivo* experiment studying the physiological role of 17β-HSD14. The molecule should therefore not behave as an agonist of the ERα. Based on their 17β-HSD14 inhibitory activity and selectivity profile toward 17β-HSD1, 17β-HSD2, and 17β-HSD10, compounds **1**, **13**, **14**, and **16** were selected to evaluate their potential agonistic effects in an estrogen receptor-dependent reporter gene assay. This assay was dose-dependently performed in U2OS-ERα cells [29] as previously described [30,31]. At the highest concentration (1000 times higher than the reference concentration of 10^{-8}M E2), the pyridine derivative **1** induced a weak agonistic response (13% compared to E2 which was set to 100%, Fig. S1, SI), while the quinoline-based inhibitors **13**, **14**, and **16** did not induce any significant estrogen-dependent response different from the control (DMSO). Quinoline-based compounds **13**, **14**, and **16** were therefore considered as better chemical probes compared to the pyridine-based **1**.

2.12. Cytotoxicity evaluation

Seven compounds (**1**, **5**, **11–14** and **16**), selected on the basis of their 17β-HSD14 inhibitory activities, were evaluated for their cytotoxic effects on the HEK293 cell line by a colorimetric assay (reduction of 3-(4,5-dimethylthiazol-2-yl)-2,5-diphenyltetrazolium bromide (MTT)) [32]. Compounds **1**, **5**, **12**, **14**, and **16** displayed a very low cytotoxicity (IG_{50}>100 μM). Due to insufficient solubility, **11** and **13** could not be tested at 100 μM, however, the cells showed 80% survival at a concentration of 20 μM, the maximally possible concentration tested (Fig. S2, SI).

3. Conclusion

The goal of this study was to develop new 17β-HSD14 inhibitors as chemical probes to further characterize the enzyme and to investigate the role of this protein. Starting from the pyridine-based inhibitor **1**, a structure-based approach was followed and 16 new inhibitors were synthesized, divided in two classes: pyridine-based and quinoline-based derivatives. The pyridine-based compounds (**1**–**8**) turned out to be highly potent (K_i of compound **5** is 1.5 nM) but non selective toward 17β-HSD1 and 17β-HSD2. The novel quinoline-based compounds (**9**–**17**) are very promising considering their potency and selectivity profiles toward 17β-HSD1, 17β-HSD2, and 17β-HSD10, especially inhibitors **13**, **14**, and **16**. Furthermore, these three compounds display no cytotoxicity in the tested cell line and do not show any significant agonistic properties. For seven of the synthesized inhibitors the crystal structures of the corresponding inhibitor-enzyme complexes were resolved. The crystal structures highlighted the binding mode of the inhibitors in the substrate binding pocket and confirmed the importance of the H-bond interactions between the catalytic Ser141 and Tyr154 and the 3-OH of the C ring inhibitor. The 3D-structures also disclosed that a small change in the substitution pattern of the compounds resulted in an alternative binding mode for one inhibitor, which would have been very difficult to predict. In addition the crystal structures have underlined the existence of several conserved water molecules, which play an important role in ligand stabilization.

Based on his potency and selectivity profile, compound **13** is suggested as a very promising tool compound and will be further investigated for metabolic stability, cell permeability, CYP-enzymes interaction, efflux pump transporters, pharmacokinetic, before potential *in vivo* use.

4. Experimental section

4.1. Chemistry

4.1.1. Chemical methods

Chemicals are named according to IUPAC nomenclature. Starting materials were used as purchased from Acros Organics, Alfa Aesar, Combi-Blocks and Sigma Aldrich without further purification. Reaction progress was monitored by TLC on aluminium sheets (Silicagel 60 F254, Merck) and visualization was accomplished with UV light. All microwave irradiation experiments were carried out in a CEM-Discover apparatus. Column chromatography was performed on silica gel (40–63 μm, Macherey-Nagel). Purification with preparative HPLC was carried out on a Varian PrepStar 218 gradient system using a ProStar 320 detector. A ProntoSIL C18 column (5.0 μm, 120 Å, 250-32 mm) was used with an acetonitrile/water gradient containing 0.1% TFA at a flow rate of 20 mL/min. All solvents were HPLC grade. Detection was performed at a wavelength of 254 nm. ^{1}H and ^{13}C NMR spectra were recorded on a Bruker AV II-300 spectrometer (at 300 MHz), a JEOL ECX-400 spectrometer (at 400 MHz and 100 MHz, respectively) and on a JEOL ECA-500 spectrometer (at 500 MHz and 125 MHz, respectively). Chemical shifts are reported in δ values (parts per million: ppm), using the hydrogenated residues of deuterated solvents as internal standard [33]: 2.05 ppm (^{1}H NMR), 29.8 ppm and 206.3 ppm (^{13}C NMR), acetone-d_6; 7.26 ppm (^{1}H NMR), 77.2 ppm (^{13}C NMR), $CDCl_3$; 2.50 ppm (^{1}H NMR), 39.5 ppm (^{13}C NMR), DMSO-d_6. Signals are described as s (singlet), bs (broad singlet), d (doublet), t (triplet), q (quartet), dd (doublet of doublet), dd (doublet of doublet of doublet), dt (doublet of triplet) and m (multiplet), respectively. All coupling constants (J) are given in Hertz (Hz). Infrared spectroscopy was performed on a Bruker ALPHA FT-IR spectrometer as neat sample. Elemental analysis was carried out on a vario MICRO elemental analyzer. Mass spectrometry was performed on a Q-Trap 2000 (Applied Biosystems) equipped with an electrospray interface (ESI). The purity of the tested compounds was evaluated by HPLC. The Shimadzu system consisted of a LC-20AT pump, an SIL-20A autosampler and a SPD-M20A PDA detector. The system was operated by the standard software LCsolution. A RP C18 NUCLEODUR (125 mm × 4 mm, 5 μm) column (Macherey-Nagel) was used as stationary phase. All solvents were HPLC grade. In a gradient run the percentage of acetonitrile (containing 0.1% trifluoroacetic acid) in water (containing 0.1% trifluoroacetic acid) was in-

creased from an initial concentration of 30% at 0 min to 90% at 15 min and kept at 90% for 5 min (HPLC-method A) or from an initial concentration of 10% at 0 min to 90% at 20 min and kept at 90% for 5 min (HPLC-method B). The injection volume was 25 μL at a flow rate of 1.00 mL/min. UV spectra were recorded at a wavelength of 254 nm. All tested compounds have ≥95% chemical purity.

The following compounds were prepared according to previously described procedures: (4-fluoro-3-methoxyphenyl)[6-(2-fluoro-3-methoxyphenyl)pyridin-2-yl]methanone (**1a**) [6], 2-bromo-6-methoxyquinoline (**12c**) [16], 7-bromoquinoline-2-carbaldehyde (**13d**) [17].

4.1.2. General procedures

4.1.2.1. General procedure for Suzuki coupling

Method A [6]

A mixture of arylbromide (1.0 eq), boronic acid (1.2 eq), cesium carbonate (4.0 eq) and tetrakis (triphenylphosphine)palladium (0.02 eq) was dissolved in DME/water (2:1), degassed and charged with argon. The mixture was stirred overnight at 80 °C. The reaction mixture was cooled down to room temperature, quenched with water and extracted with ethyl acetate. The combined organic layers were washed with brine, dried over magnesium sulfate, filtered and evaporated to dryness under reduced pressure. The crude product was purified by column chromatography.

4.1.2.2. General procedures for ether cleavage

Method B1 [6]

A solution of methoxy derivative (1.0 eq) in dry dichloromethane was cooled down to −80 °C and boron tribromide (1.0 M in dichloromethane, 5.0 eq per methoxy function) was slowly added under argon. The reaction mixture was stirred at −80 °C for 1 h and then allowed to warm to room temperature overnight. The mixture was cooled down with an ice bath, quenched with water and extracted with ethyl acetate. The combined organic layers were washed with brine, dried over magnesium sulfate, filtered and evaporated to dryness under reduced pressure. The crude product was purified by column chromatography.

Method B2 [34]

To a solution of methoxy derivative (1.0 eq) in anhydrous dichloromethane, boron trifluoride dimethylsulfide complex (35 eq per methoxy function) was added dropwise under argon and the reaction mixture was stirred at room temperature overnight. The mixture was quenched with water and extracted with dichloromethane or ethyl acetate. The combined organic layers were washed with brine, dried over magnesium sulfate, filtered and evaporated to dryness under reduced pressure. The crude product was purified by column chromatography or preparative HPLC.

4.1.2.3. General procedure for N-methylation

Method C

A solution of amide derivative (1.0 eq) in DMF was cooled down to 0 °C and sodium hydride (60% w/w, 1.5 eq) was added. The mixture was warmed to room temperature for 20 min and cooled down again to 0 °C. Iodomethane (2.0 eq) was added and the reaction mixture was stirred at room temperature. The end of the reaction was monitored by TLC. Water was added to quench the reaction and the aqueous layer was extracted with ethyl acetate. The combined organic layers were washed with brine, dried over magnesium sulfate, filtered and evaporated to dryness under reduced pressure. The crude product was purified by silica gel column chromatography.

4.1.2.4. General procedure for amide formation

Method D

A solution of carboxylic acid derivative (1.0 eq, 0.2 M), thionyl chloride (2.0 eq) and DMF (catalytic amount) in toluene was refluxed at 110 °C for 4 h under argon atmosphere. The mixture was cooled down to room temperature and the solvent as well as the excess of thionyl chloride were removed under reduced pressure. The residue (0.2 M) was dissolved in dry dichloromethane and the appropriate amine (1.0 eq) as well as trimethylamine (1.0 eq) were added at 0 °C under argon atmosphere. The reaction mixture was stirred at room temperature overnight. The solvent was evaporated to dryness under reduced pressure and the residue was taken up in ethyl acetate. The organic layer was washed with 0.5 M hydrochloric acid, saturated sodium bicarbonate and brine, dried over magnesium sulfate, filtered and evaporated to dryness under reduced pressure. The crude product was purified by silica gel column chromatography.

4.1.2.5. General procedures for alcohol formation

Method E1 [6]

A solution of *n*-BuLi (1.0 eq, 2.5 M in hexane) was diluted with anhydrous THF to a final concentration of 0.8 M and arylbromide (1.0 eq) in anhydrous THF was slowly added at −80 °C under argon. The resulting solution was stirred for 15 min at −80 °C. A solution of the appropriate aldehyde (1.0–1.1 eq) in anhydrous THF was added and the reaction solution was stirred for additional 15 min at −80 °C and at room temperature for 2 h under argon. The mixture was quenched with saturated ammonium chloride and extracted with ethyl acetate. The combined organic layers were washed with brine, dried over magnesium sulfate, filtered and evaporated to dryness under reduced pressure. The product was purified by column chromatography.

Method E2

A mixture of arylbromide (1.0 eq), magnesium turnings (1.1 eq) and a catalytic amount of iodine in anhydrous THF was stirred for 2 h at 60 °C under argon. A solution of the appropriate aldehyde in anhydrous THF was added and the reaction mixture was stirred at 80 °C. The end of the reaction was monitored by TLC. The mixture was quenched with brine and extracted with ethyl acetate. The combined organic layers were dried over magnesium sulfate, filtered and evaporated to dryness under reduced pressure. The crude product was purified by column chromatography.

4.1.2.6. General procedure for alcohol oxidation

Method F [6]

2-Iodoxybenzoic acid (1.2 eq) was added to a solution of alcohol derivative (1.0 eq) in THF and the reaction mixture was stirred at 60 °C. After the end of the reaction (monitored by TLC) the mixture was cooled to room temperature, quenched with saturated sodium thiosulfate and extracted with ethyl acetate. The combined organic layers were washed with water and saturated sodium bicarbonate, dried over magnesium sulfate, filtered and evaporated to dryness under reduced pressure. The crude product was purified by column chromatography.

4.1.3. Detailed synthesis procedures of selected compounds

4.1.3.1. (7-Bromoquinolin-2-yl) (4-fluoro-3-methoxyphenyl)methanol (13c)

According to **method E2** the title compound was prepared by reaction of 4-bromo-1-fluoro-2-methoxybenzene (**13e**) (5.27 g, 25.7 mmol, 1.2 eq) with 7-bromoquinoline-2-carbaldehyde (**13d**) [17] (5.05 g, 21.4 mmol, 1.0 eq). The crude product was used in the next step without further purification. C17H13BrFNO2; MW: 362; **MS** (ESI): 362, 364 (M + H)+.

4.1.3.2. (7-Bromoquinolin-2-yl) (4-fluoro-3-methoxyphenyl)methanone (13b)

According to **method F** the title compound was prepared by reaction of the previously obtained (7-bromoquinolin-2-yl) (4-fluoro-3-methoxy-phenyl)methanol (**13c**) with 2-iodoxybenzoic acid (7.20 g, 25.7 mmol, 1.2 eq) overnight. The crude product was washed with methanol to give 5.96 g (16.5 mmol, 77%, two steps) of the analytically pure compound. $C_{17}H_{11}BrFNO_2$; MW 360; **^{1}H NMR** ($CDCl_3$, 400 MHz): δ 8.39–8.38 (m, 1H), 8.33 (d, J = 8.5 Hz, 1H), 8.11 (d, J = 8.5 Hz, 1H), 7.95 (dd, J = 8.4 Hz, 2.0 Hz, 1H), 7.87 (dd, J = 8.4 Hz, 4.5 Hz, 2.0 Hz, 1H), 7.80–7.73 (m, 2H), 7.18 (dd, J = 10.7 Hz, 8.5 Hz, 1H), 3.98 (s, 3H); **^{13}C NMR** ($CDCl_3$, 100 MHz): δ 191.6, 156.0 (d, J = 256.1 Hz), 155.4, 147.8 (d, J = 11.1 Hz), 147.2, 137.4 (d, J = 1.3 Hz), 132.7, 132.4 (d, J = 3.6 Hz), 132.2, 129.0, 127.6, 126.3 (d, J = 8.1 Hz), 124.6 (d, J = 1.3 Hz), 121.4, 115.8 (d, J = 3.5 Hz), 115.8 (d, J = 19.2 Hz), 56.5; **MS** (ESI): 360, 362 $(M + H)^+$.

4.1.3.3. 2 -(4-Fluoro-3-methoxybenzoyl)quinoline-7-carbonitrile (13a)

A mixture of (7-bromoquinolin-2-yl) (4-fluoro-3-methoxyphenyl)-methanone (**13b**) (180 mg, 0.50 mmol, 1.0 eq), zinc cyanide (59 mg, 0.50 mmol, 1.0 eq) and tetrakis (triphenylphosphine)palladium (17 mg, 0.02 mmol, 0.03 eq) in dimethylformamide (2.5 mL) was degassed and charged with argon. The mixture was stirred for 3 h at 120 °C. The reaction mixture was cooled down to room temperature, diluted with ethyl acetate and washed with water and brine. The organic layers were dried over magnesium sulfate, filtered and evaporated to dryness under reduced pressure. The crude product was purified by column chromatography (neat dichloromethane) to give 105 mg (0.34 mmol, 69%) of the analytically pure compound. $C_{18}H_{11}FN_2O_2$, MW: 306; **^{1}H NMR** ($CDCl_3$, 400 MHz): δ 8.57–8.56 (m, 1H), 8.42 (dd, J = 8.6 Hz, 0.6 Hz, 1H), 8.24 (d, J = 8.6 Hz, 1H), 8.03 (d, J = 8.4 Hz, 1H), 7.95 (dd, J = 8.3 Hz, 2.0 Hz, 1H), 7.88 (dd, J = 8.4 Hz, 4.5 Hz, 2.1 Hz, 1H), 7.82 (dd, J = 8.5 Hz, 1.6 Hz, 1H), 7.20 (dd, J = 10.7 Hz, 8.5 Hz, 1H), 3.99 (s, 3H); **^{13}C NMR** ($CDCl_3$, 100 MHz): 191.2 (d, J = 1.3 Hz), 156.4, 156.2 (d, J = 256.7 Hz), 148.0 (d, J = 11.1 Hz), 145.6, 137.5, 136.3, 132.1 (d, J = 3.7 Hz), 130.9, 129.4, 129.2, 126.4 (d, J = 8.2 Hz), 123.6, 118.2, 115.9 (d, J = 18.9 Hz), 115.7 (d, J = 3.6 Hz), 114.1, 56.5; **MS** (ESI): 307 $(M + H)^+$.

4.1.3.4. 2 -(4-Fluoro-3-hydroxybenzoyl)quinoline-7-carbonitrile (13)

According to **method B1** the title compound was prepared by reaction of 2-(4-fluoro-3-methoxybenzoyl)quinoline-7-carbonitrile **(13a)** (92 mg, 0.3 mmol, 1.0 eq) with boron tribromide (1.5 mL, 1.5 mmol, 5.0 eq) in dichloromethane (6.0 mL). The product was purified by column chromatography (cyclohexane/ethyl acetate 2:1 → 1:1) and preparative HPLC (gradient water/acetonitrile/trifluoroacetic acid 70:30:0.1 → 10:90:0.1 in 120 min) to give 53 mg (0.18 mmol/60%) of the analytically pure compound. $C_{17}H_9FN_2O_2$; MW: 292; **mp**: 222–223 °C; **^{1}H NMR** (acetone-d_6, 500 MHz): δ 9.09 (bs, 1H), 8.71 (d, J = 8.6 Hz, 1H), 8.63 (dd, J = 1.5 Hz, 0.7 Hz, 1H), 8.31 (d, J = 8.5 Hz, 1H), 8.21 (d, J = 8.6 Hz, 1H), 8.01–7.97 (m, 2H), 7.81 (dd, J = 8.5 Hz, 4.5 Hz, 2.2 Hz, 1H), 7.29 (dd, J = 10.8 Hz, 8.5 Hz, 1H); **^{13}C NMR** (acetone-d_6, 125 MHz): δ 191.8, 157.5, 155.8 (d, J = 250.2 Hz), 146.2, 145.6 (d, J = 13.5 Hz), 138.7, 136.6, 133.5 (d, J = 3.5 Hz), 131.8, 130.7, 129.9, 125.2 (d, J = 7.8 Hz), 123.9, 121.5 (d, J = 4.7 Hz), 118.8, 116.8 (d, J = 19.3 Hz), 114.6; **IR**: 3066, 3035, 2236, 1674, 1323, 864 cm^{-1}; **MS** (ESI): 293 $(M + H^+)$; **Elemental analysis** calculated (%) for $C_{17}H_9FN_2O_2 \cdot 0.8H_2O$: C 66.58, H 3.48, N 9.13. Found: C 66.44, H 3.27, N 9.15; **HPLC** analysis: retention time = 11.82 min; peak area, 99.9%, HPLC-method A.

4.2. Biological methods

4.2.1. 17β-HSD14 enzyme expression and purification

The pure recombinant 17β-HSD14 enzyme was obtained via heterologous expression using a p11-Toronto1 vector and the competent cells BL21 *pLysS* strain of *E coli* as previously described [3,6]. The protein purification was performed applying two steps of affinity chromatography (Ni-NTA column) followed by size-exclusion chromatography. The stability of the protein was increased by addition of the cofactor (NAD^+) and of 250 mM glucose to the buffer during purification and storage. Purity was confirmed by SDS page and mass spectrometry (results not shown).

4.2.2. Inhibition of 17β-HSD14

Inhibitory activities were evaluated with a fluorimetric assay following the already described protocol [6], using the purified, recombinantly expressed enzyme, E2 as substrate, NAD^+ as cofactor, and the inhibitors. A high enzyme concentration (between 2.2 μM and 3.4 μM) and high substrate concentration (E2 = 32 μM) had to be used because of the low sensitivity of the assay. As the inhibitor concentration studied was in the same range as the enzyme concentration used, no classical kinetic analysis could be applied for the determination of K_i [35,36]. The data were analyzed using the quadratic Morrison equation for tight binding inhibitors [37].

Briefly, to a mixture of NAD^+ (1.2 mM) and E2 (32 μM) in 100 mM phosphate buffer pH 8, the potential inhibitor was added in DMSO (final DMSO concentration in assay: 1%) and the enzymatic reaction was started by addition of the purified enzyme (1 mg/mL). The production of the fluorescent NADH formed was measured continuously for 15 min on a Tecan Saphire 2. A linear relationship between product formation and reaction time was obtained and the slope of the progress curves was calculated by linear regression. The K_i values were calculated by means of the Morrison equation using the procedure detailed by Copeland [22] as previously described [6]. The fitting and data analysis were performed using GraphPad Prism 7.

4.2.3. Inhibition of 17β-HSD1 and 17β-HSD2

17β-HSD1 and 17β-HSD2 were partially purified from human placenta according to previously described procedures [27,,38]. For the 17β-HSD1 inhibition assay the cytosolic fraction was incubated with [NADH] = 500 μM, and the potential inhibitor was added in DMSO (final concentration in assay: 1 μM, final DMSO concentration: 1%) at 37 °C in a phosphate buffer (50 mM, pH 7.4). The enzymatic reaction was started by addition of the radioactive [2,4,6,7-^{3}H]-E1 in a mixture with the unlabeled substrate E1 (final concentration: 500 nM) and stopped with $HgCl_2$ after 10 min. Separation and quan-

tification of the extracted radioactive steroids were performed by HPLC coupled to a radioflow detector. The 17β-HSD2 inhibition assay was performed similarly incubating the microsomal fraction in the presence of [NAD^+] = 1500 μM and [2,4,6,7-^{3}H]-E2 in a mixture with the unlabeled substrate E2 (final concentration: 500 nM).

4.2.4. Cloning and expression of recombinant human 17β-HSD10

The full length coding DNA sequence of human 17β-HSD10 (according to data base entry NM_004493.2 without the start codon ATG) was amplified from HeLa cDNA using the forward primer 5′-TTTGGATCCGCAGCAGCGTGTCGGAGCG-3′ and the reverse primer 5′-TTTGAGCTCAAGGCTGCATACGAATGGC-3′ and cloned into a modified pGex vector (constructed from pGex-2T (Qiagen) by Leenders et al. [39]). Sequence correctness was verified by Sanger sequencing. *N*-terminally GST-tagged 17β-HSD10 enzyme was expressed in *E coli* BL21 DE3 Codon Plus RP (Stratagene).

4.2.5. Inhibition of 17β-HSD10

A suspension of the bacterial pellet in 100 mM phosphate buffer pH 7.7 was incubated with [6,7-^{3}H]-E2 (final concentration: 25 nM) in presence of the potential inhibitor in DMSO (final concentration in assay: 1 μM, final DMSO concentration: 1%) at 37 °C. The enzymatic reaction was started by addition of NAD^+ (0.75 mM) and stopped by means of 0.21 M ascorbic acid in a methanol/acetic acid mixture (99:1, v/v) after an incubation time of 30 min. Substrate and product were extracted from the reaction mixture by SPE (Strata C18-E columns from Phenomenex on a vacuum device). Separation and quantification of the radioactive labeled steroids were performed with HPLC (Luna 5 μm C18 (2), 125 × 4.00 mm from Phenomenex, with an acetonitrile/water mixture (43:57, v/v), flow rate 1 mL/min). Substrate conversion is given in % as calculated after integration of the product and substrate peaks. Inhibition was calculated based on conversion without potential inhibitor (DMSO only) which was set to 0% inhibition.

4.2.6. Solubility

The solubility range of most of the compounds was determined by mixing a solution of the studied inhibitors in DMSO at several concentrations in 100 mM phosphate buffer at pH 7.4 (final DMSO concentration: 2%) and visually assessing the precipitation status at different time points (0, 1, 2 and 24 h).

4.2.7. Reporter gene assay in U2OS-ERα cells

The assay was performed in U2OS-ERα cells, a generous gift from Dr. Monroe [29] as previously described [30,31]. The cells were pre-cultured in DMEM/F12 medium containing 10% fetal calf serum (FCS) and 250 μg/mL zeocin and 2.5 μg/mL blasticidin. Experiments were performed with DMEM/F12 medium containing 5% dextran coated charcoal (DCC) stripped FCS and, 100 ng/mL doxycycline for ERα expression. U2OS-ERα cells at a density of 80,000 cells per well (24-well plate) were transfected with 0.4 μg of the $(ERE)_2$-tk-Luc reporter plasmid using Attractene Transfection Reagent (ATR, Qiagen). Cells were treated 24 h after transfection with the test compounds. All test compounds were dissolved in DMSO and added in a way that the DMSO concentration in the test did not exceed 0.1%. As controls, cells were treated either with 0.1% DMSO (negative control) or 10^{-8} M E2 (positive control). Cells were harvested 24 h after treatment; luciferase activity was measured with a commercial kit (Promega, Mannheim, Germany) and total protein content was measured using a bicinchoninic acid (BCA) protein assay. Luciferase activity was calculated in relative luciferase units (RLU) per mg of protein. Experiments were conducted three times with technical triplicates. Statistical analysis was performed using a paired *t-test*. A probability of <0.05 was defined as significant. *$p < 0.05$, **$p < 0.01$, compared to the solvent control.

4.2.8. Cytotoxicity assay

Potential cytotoxicity of inhibitors **1**, **13**, **14**, and **16** toward HEK293 cells was determined by an MTT assay [32] as previously described [40]. The cells were seeded into 96-well plates overnight at a 1×10^4 cells/well density. Series of inhibitor concentrations (from 0 to 100 μM) were added to the wells and incubated for 72 h, at 37 °C under 5% CO_2. The cell viability was subsequent evaluated by the MTT colorimetric assay.

4.3. Crystallography: co-crystallization of the protein with inhibitors

The co-crystallization of 17β-HSD14 in complex with the cofactor NAD^+ and the different classes of inhibitors was performed following the already described and optimized protocols [3,6].

The final inhibitor concentration of 4 mM was incubated with the protein solution (9.5 mg/mL) containing 0.6 mM NAD^+ and 5% DMSO for 30 min. The mixture was then centrifuged at 10,000 *g* for 20 min in order to separate the precipitant. Afterwards, 2 μL of the supernatant was mixed with 2 μL of mother liquor composed of 0.1 M HEPES, 20% (w/v) PEG6000 and 5% (v/v) DMSO, adjusted to pH 7.0. Crystals of sufficient quality for data collection were grown at a temperature of 18 °C for 10 days and then exposed for a few seconds to a cryo buffer obtained by the combination of mother liquor with the addition of glucose (20% v/v) and of the respective inhibitors (4 mM final concentration). Finally, the specimens were successively flash-frozen in liquid nitrogen. Diffraction data have been collected on BL14.1 at the BESSY II electron storage ring operated by the Helmholtz-Zentrum Berlin [41]. Data collection, processing and structure determination details can be found in the supporting information (Table S2A and B).

4.4. MOE models

The inhibitors **9**, **12**, **14**, **15** and **17** were modeled inside the crystal structure (PDB code: 5L7Y [3]) by removing the parent ligand **1** and minimized with MOE [42]. During minimization, the AMBER12 force field was applied. The heavy atoms of the protein and the 3-OH group at the C ring of the inhibitors were fixed to maintain the direct interaction with Tyr154 resulting in the most prominent binding mode observed for the inhibitors described for 17β-HSD14. In order to give the ligand sufficient freedom to move, the residues His93, Gln148 and Met199 were also allowed to move unrestricted during minimization.

Associated content

Supporting information

Chemistry: Chemical methods, General procedures, Detailed synthesis procedures; Physicochemical properties; Crystallography: Data collection and processing, Crystallographic table, Structure determination and refinement; Reporter gene assay in U2OS-ERα cells; Cytotoxicity evaluation; MOE models.

Accession code

Atomic coordinates and experimental data for the co-crystal structures of **2** (PDB code: 5O6O), **4** (PDB code: 5O43), **5** (PDB code:

5O42), **9** (PDB code: 5O6Z), **11** (PDB code: 5O6X), **13** (PDB code: 5O7C), and **16** (PDB code: 5O72) in complex with 17β-HSD14 will be released upon article publication.

Declaration of interest

The authors declare no competing financial interest.

Abbreviations

17β-HSD14, 17β-hydroxysteroid dehydrogenase type 14; 17β-HSD1, 17β-hydroxysteroid dehydrogenase type 1; 17β-HSD2, 17β-hydroxysteroid dehydrogenase type 2; 17β-HSD10, 17β-hydroxysteroid dehydrogenase type 10; SDR, short-chain dehydrogenase reductase; E2, estradiol; 5-diol, 5-androstene-3β,17β-diol; E1, estrone; ER, estrogen receptor; SAR, structure activity relationship; PPPM, phenyl(6-phenyl)pyridin-2-yl methanone; DHEA, dehydroepiandrosterone, LHMDS, lithium hexamethyldisilazane ; DCM, dichloromethane; H-bond, hydrogen bond.

Acknowledgments

The authors are grateful to the Deutsche Forschungsgemeinschaft (DFG) (MA-5287/1-1 and KL-1204/15-1), the Partenariats Hubert Curien (PHC) (Campus France, Programme Procop, 35498NF) and the Deutscher Akademischer Austauschdienst (PPP Frankreich 1j 16, 57207471) for financial support. Diffraction data have been collected on BL14.1 at the BESSY II electron storage ring operated by the Helmholtz-Zentrum Berlin. We would particularly like to acknowledge the help and support of beam line scientist during the experiments. We are also thankful to Helmholtz-Zentrum Berlin (HZB) for their financial support. We also thank M. Jud Badran and Erik Kerste, Andreas Schmidt and Matthias Tripp for their help during their internships. We acknowledge Janine Ludwig for performing the 17β-HSD1 and 17β-HSD2 inhibition assays. We are also grateful to ChemAxon Ltd. for providing free access to Marvin Sketch 15.9.14 for the pK_a calculations and to Dr. Peter Ertl for providing the free access to the PAINS-remover tool.

Appendix A. Supplementary data

Supplementary data related to this article can be found at https://doi.org/10.1016/j.ejmech.2018.05.029.

Uncited references

[40].

References

[1] P. Lukacik, K.L. Kavanagh, U. Oppermann, Structure and function of human 17β-hydroxysteroid dehydrogenases, Mol. Cell. Endocrinol. 248 (2006) 61–71, https://doi.org/10.1016/j.mce.2005.12.007.
[2] P. Lukacik, B. Keller, G. Bunkoczi, K.L. Kavanagh, W. Hwa Lee, J. Adamski, U. Oppermann, W.H. Lee, W. Hwa Lee, J. Adamski, U. Oppermann, Structural and biochemical characterization of human orphan DHRS10 reveals a novel cytosolic enzyme with steroid dehydrogenase activity, Biochem. J. 402 (2007) 419–427, https://doi.org/10.1042/BJ20061319.
[3] N. Bertoletti, F. Braun, M. Lepage, G. Möller, J. Adamski, A. Heine, G. Klebe, S. Marchais-Oberwinkler, New insights into human 17β-hydroxysteroid dehydrogenase type 14: first crystal structures in complex with a steroidal ligand and with a potent nonsteroidal inhibitor, J. Med. Chem. 59 (2016) 6961–6967, https://doi.org/10.1021/acs.jmedchem.6b00293.
[4] T. Sivik, S. Vikingsson, H. Gréen, A. Jansson, Expression patterns of 17β-hydroxysteroid dehydrogenase 14 in human tissues, Horm. Metab. Res. 44 (2012) 949–956, https://doi.org/10.1055/s-0032-1321815.
[5] F. Haeseleer, K. Palczewski, Short-chain dehydrogenases/reductases in retina, 316 (2000) 372–383.
[6] F. Braun, N. Bertoletti, G. Möller, J. Adamski, T. Steinmetzer, M. Salah, A.S. Abdelsamie, C.J. van Koppen, A. Heine, G. Klebe, S. Marchais-Oberwinkler, First structure–activity relationship of 17β-hydroxysteroid dehydrogenase type 14 nonsteroidal inhibitors and crystal structures in complex with the enzyme, J. Med. Chem. 59 (2016) 10719–10737, https://doi.org/10.1021/acs.jmedchem.6b01436.
[7] G.L. Patrick, An Introduction to Medicinal Chemistry, fifth ed., Oxford University Press, Oxford, 2013.
[8] The PyMOL Molecular Graphics System, Version 1.7.X, Schrödinger, LLC.
[9] J.B. Baell, G.A. Holloway, New substructure filters for removal of pan assay interference compounds (PAINS) from screening libraries and for their exclusion in bioassays, J. Med. Chem. 53 (2010) 2719–2740, https://doi.org/10.1021/jm901137j.
[10] http://cbligand.org/PAINS/search_struct.php, 15.11.2016. (Accessed 15 November 2016).
[11] D.F. Veber, S.R. Johnson, H.-Y. Cheng, B.R. Smith, K.W. Ward, K.D. Kopple, Molecular properties that influence the oral bioavailability of drug candidates, J. Med. Chem. 45 (2002) 2615–2623, https://doi.org/10.1021/jm020017n.
[12] C.A. Lipinski, F. Lombardo, B.W. Dominy, P.J. Feeney, Experimental and computational approaches to estimate solubility and permeability in drug discovery and development settings, Adv. Drug Deliv. Rev. 46 (2001) 3–26.
[13] H. Pajouhesh, G.R. Lenz, Medicinal chemical properties of successful central nervous system drugs, NeuroRx 2 (2005) 541–553.
[14] N. Miyaura, A. Suzuki, Palladium-catalyzed cross-coupling reactions of organoboron compounds, Chem. Rev. 95 (1995) 2457–2483, https://doi.org/10.1021/cr00039a007.
[15] G. Wittig, G. Geissler, Zur Reaktionsweise des Pentaphenyl-phosphors und einiger Derivate, Justus Liebigs Ann. Chem. 580 (1953) 44–57, https://doi.org/10.1002/jlac.19535800107.
[16] S.E. Wengryniuk, A. Weickgenannt, C. Reiher, N.A. Strotman, K. Chen, M.D. Eastgate, P.S. Baran, Regioselective bromination of fused heterocyclic N-oxides, Org. Lett. 15 (2013) 792–795, https://doi.org/10.1021/ol3034675.
[17] M. Petit, G. Bort, B.-T. Doan, C. Sicard, D. Ogden, D. Scherman, C. Ferroud, P.I. Dalko, X-ray photolysis to release ligands from caged reagents by an intramolecular antenna sensitive to magnetic resonance imaging, Angew. Chem. Int. Ed. 50 (2011) 9708–9711, https://doi.org/10.1002/anie.201102948.
[18] M. Alterman, A. Hallberg, Fast microwave-assisted preparation of aryl and vinyl nitriles and the corresponding tetrazoles from organo-halides, J. Org. Chem. 65 (2000) 7984–7989, https://doi.org/10.1021/jo0009954.
[19] X. Zeng, W. Huang, Y. Qiu, S. Jiang, An efficient copper-catalyzed synthesis of anilines by employing aqueous ammonia, Org. Biomol. Chem. 9 (2011) 8224–8227, https://doi.org/10.1039/C1OB06208E.
[20] UniProt: the universal protein knowledgebase, Nucleic Acids Res. 45 (2017) D158–D169, https://doi.org/10.1093/nar/gkw1099.
[21] C.R. Kissinger, P.A. Rejto, L.A. Pelletier, J.A. Thomson, R.E. Showalter, M.A. Abreo, C.S. Agree, S. Margosiak, J.J. Meng, R.M. Aust, D. Vanderpool, B. Li, A. Tempczyk-Russell, J.E. Villafranca, Crystal structure of human ABAD/HSD10 with a bound inhibitor: implications for design of Alzheimer's disease therapeutics, J. Mol. Biol. 342 (2004) 943–952, https://doi.org/10.1016/j.jmb.2004.07.071.
[22] G. Neudert, G. Klebe, fconv: format conversion, manipulation and feature computation of molecular data, Bioinformatics 27 (2011) 1021–1022, https://doi.org/10.1093/bioinformatics/btr055.
[23] J.W. Lustbader, M. Cirilli, C. Lin, H.W. Xu, K. Takuma, N. Wang, C. Caspersen, X. Chen, S. Pollak, M. Chaney, F. Trinchese, S. Liu, F. Gunn-Moore, L.-F. Lue, D.G. Walker, P. Kuppusamy, Z.L. Zewier, O. Arancio, D. Stern, S.S. Yan, H. Wu, ABAD directly links Abeta to mitochondrial toxicity in Alzheimer's disease, Science 304 (2004) 448–452, https://doi.org/10.1126/science.1091230.
[24] F. Braun, N. Bertoletti, G. Möller, J. Adamski, T. Steinmetzer, M. Salah, A.S. Abdelsamie, C.J. van Koppen, A. Heine, G. Klebe, S. Marchais-Oberwinkler, First structure-activity relationship of 17β-hydroxysteroid dehydrogenase type 14 nonsteroidal inhibitors and crystal structures in complex with the enzyme, J. Med. Chem. 59 (2016) 10719–10737, https://doi.org/10.1021/acs.jmedchem.6b01436.
[25] S. Marchais-Oberwinkler, C. Henn, G. Möller, T. Klein, M. Negri, A. Oster, A. Spadaro, R. Werth, M. Wetzel, K. Xu, M. Frotscher, R.W. Hartmann, J. Adamski, 17β-Hydroxysteroid dehydrogenases (17β-HSDs) as therapeutic targets: protein structures, functions, and recent progress in inhibitor development, J. Steroid Biochem. Mol. Biol. 125 (2011) 66–82, https://doi.org/10.1016/j.jsbmb.2010.12.013.
[26] P. Kruchten, R. Werth, S. Marchais-Oberwinkler, M. Frotscher, R.W. Hartmann, Development of a biological screening system for the evaluation of highly active

and selective 17beta-HSD1-inhibitors as potential therapeutic agents, Mol. Cell. Endocrinol. 301 (2009) 154–157, https://doi.org/10.1016/j.mce.2008.09.035.
[27] P. Kruchten, Development of a Screening System for the Identification of Highly Active and Selective Inhibitors of 17beta-hydroxysteroid-dehydrogenase Type 1 (17betaHSD1), Dissertation Saarland University, 2009https://doi.org/10.22028/D291-22614.
[28] C. Yung-Chi, W.H. Prusoff, Relationship between the inhibition constant (KI) and the concentration of inhibitor which causes 50 per cent inhibition (I50) of an enzymatic reaction, Biochem. Pharmacol. 22 (1973) 3099–3108, https://doi.org/10.1016/0006-2952(73)90196-2.
[29] D.G. Monroe, B.J. Getz, S.A. Johnsen, B.L. Riggs, S. Khosla, T.C. Spelsberg, Estrogen receptor isoform-specific regulation of endogenous gene expression in human osteoblastic cell lines expressing either ERα or ERβ, J. Cell. Biochem. 90 (2003) 315–326, https://doi.org/10.1002/jcb.10633.
[30] F. Möller, O. Zierau, A. Jandausch, R. Rettenberger, M. Kaszkin-Bettag, G. Vollmer, Subtype-specific activation of estrogen receptors by a special extract of Rheum rhaponticum (ERr 731®), its aglycones and structurally related compounds in U2OS human osteosarcoma cells, Phytomedicine 14 (2007) 716–726, https://doi.org/10.1016/j.phymed.2007.09.001.
[31] J. Wober, F. Möller, T. Richter, C. Unger, C. Weigt, A. Jandausch, O. Zierau, R. Rettenberger, M. Kaszkin-Bettag, G. Vollmer, Activation of estrogen receptor-beta by a special extract of Rheum rhaponticum (ERr 731), its aglycones and structurally related compounds, J. Steroid Biochem. Mol. Biol. 107 (2007) 191–201, https://doi.org/10.1016/j.jsbmb.2007.04.002.
[32] T. Mosmann, Rapid colorimetric assay for cellular growth and survival: application to proliferation and cytotoxicity assays, J. Immunol. Meth. 65 (1983) 55–63.
[33] H.E. Gottlieb, V. Kotlyar, A. Nudelman, NMR chemical shifts of common laboratory solvents as trace impurities, J. Org. Chem. 62 (1997) 7512–7515, https://doi.org/10.1021/jo971176v.
[34] M. Wetzel, E.M. Gargano, S. Hinsberger, S. Marchais-Oberwinkler, R.W. Hartmann, Discovery of a new class of bicyclic substituted hydroxyphenyl-methanones as 17β-hydroxysteroid dehydrogenase type 2 (17β-HSD2) inhibitors for the treatment of osteoporosis, Eur. J. Med. Chem. 47 (2012) 1–17, https://doi.org/10.1016/j.ejmech.2011.09.004.
[35] J.F. Morrison, The slow-binding and slow, tight-binding inhibition of enzyme-catalysed reactions, Trends Biochem. Sci. 7 (1982) 102–105, https://doi.org/10.1016/0968-0004(82)90157-8.
[36] J.F. Morrison, Kinetics of the reversible inhibition of enzyme-catalysed reactions by tight-binding inhibitors, Biochim. Biophys. Acta 185 (1969) 269–286.
[37] R.A. Copeland, Enzymes: a Practical Introduction to Structure, Mechanism, and Data Analysis, second ed., Wiley-VCH, New York, 2000.
[38] K.M. Sam, R.P. Boivin, M.R. Tremblay, S. Auger, D. Poirier, C16 and C17 derivatives of estradiol as inhibitors of 17 beta-hydroxysteroid dehydrogenase type 1: chemical synthesis and structure-activity relationships, Drug Des. Discov. 15 (1998) 157–180.
[39] F. Leenders, J.G. Tesdorpf, M. Markus, T. Engel, U. Seedorf, J. Adamski, Porcine 80-kDa protein reveals intrinsic 17-hydroxysteroid dehydrogenase, fatty acyl-CoA-hydratase/dehydrogenase, and sterol transfer activities, J. Biol. Chem. 271 (1996) 5438–5442, https://doi.org/10.1074/jbc.271.10.5438.
[40] A. do, R.A. Pires, F. Lecerf-Schmidt, N. Guragossian, J. Pazinato, G.J. Gozzi, E. Winter, G. Valdameri, A. Veale, A. Boumendjel, A. Di Pietro, B. Pérès, New, highly potent and non-toxic, chromone inhibitors of the human breast cancer resistance protein ABCG2, Eur. J. Med. Chem. 122 (2016) 291–301, https://doi.org/10.1016/j.ejmech.2016.05.053.
[41] U. Mueller, N. Darowski, M.R. Fuchs, R. Förster, M. Hellmig, K.S. Paithankar, S. Pühringer, M. Steffien, G. Zocher, M.S. Weiss, Facilities for macromolecular crystallography at the Helmholtz-Zentrum Berlin, J. Synchrotron Radiat. 19 (2012) 442–449, https://doi.org/10.1107/S0909049512006395.
[42] Molecular Operating Environment (MOE), 2013.08; Chemical Computing Group Inc., 1010 Sherbooke St. West, Suite #910, Montreal, QC, Canada, H3A 2R7, 2016., (n.d.).